POLYPUBLIE

Multi-IRS-Aided Terahertz Networks: Channel Modeling and User Association With Imperfect CSI

Muddasir Rahim, Thanh Luan Nguyen, Georges Kaddoum, Tri Nhu Do

Document en libre accès dans PolyPublie
Open Access document in PolyPublie

Date	2024
Type	Article de revue / Article
Version	Version officielle de l'éditeur / Published version
URL de PolyPublie PolyPublie URL	https://publications.polymtl.ca/57484/
Évaluation par les pairs Peer reviewed	Révisé par les pairs / Refereed
Conditions d'utilisation Terms of use	Creative Commons Attribution-Utilisation non commerciale-Pas d'oeuvre dérivée 4.0 International / Creative Commons Attribution-NonCommercial-NoDerivatives 4.0 International (CC BY-NC-ND)
Référence Citation	Rahim, M., Nguyen, T. L., Kaddoum, G., & Do, T. N. (2024). Multi-IRS-Aided Terahertz Networks: Channel Modeling and User Association With Imperfect CSI. IEEE Open Journal of the Communications Society, 5, 836-855. https://doi.org/10.1109/ojcoms.2024.3353173

Publication officielle
Official publication

Titre de la revue Journal title	IEEE Open Journal of the Communications Society (vol. 5)
Maison d'édition Publisher	IEEE
URL officielle Official URL	https://doi.org/10.1109/ojcoms.2024.3353173
Mention légale Legal notice	

Ce fichier a été téléchargé à partir de PolyPublie, le dépôt institutionnel de Polytechnique Montréal
This file has been downloaded from PolyPublie, the institutional repository of Polytechnique Montréal
https://publications.polymtl.ca

This article has been accepted for publication in IEEE Open Journal of the Communications Society. This is the author's version which has not been fully edited and content may change prior to final publication. Citation information: DOI 10.1109/OJCOMS.2024.3353173

Multi-IRS-aided Terahertz Networks: Channel Modelling and User Association With Imperfect CSI

Muddasir Rahim*, Thanh Luan Nguyen*, Georges Kaddoum**, *Senior Member, IEEE*, and Tri Nhu Do†

***Abstract*—Terahertz (THz) communication is envisioned as one of the candidate technologies for future wireless communications to enable achievable data rates of up to several terabits per second (Tbps). However, the high pathloss and molecular absorption in THz band communications often limit the transmission range. To overcome these limitations, this paper proposes intelligent reconfigurable surface (IRS)-aided THz networks with imperfect channel state information (CSI). Specifically, we present an angle-based trigonometric channel model to facilitate the performance evaluation of IRS-aided THz networks. In addition, to maximize the sum rate, we formulate the transmitter (Tx)-IRS-receiver (Rx) matching problem, which is a mixed-integer nonlinear programming (MINLP) problem. To address this non-deterministic polynomial-time hard (NP-hard) problem, we propose a Gale-Shapley algorithm-based solutions to obtain stable matching between transmitters and IRSs, and receivers and IRSs, in the first and second sub-problems, respectively. The impact of the transmission power, the number of IRS elements, and the network area on the sum rate are investigated. Furthermore, the proposed algorithm is compared to an exhaustive search, nearest association, greedy search, and random allocation to validate the proposed solution. The complexity and convergence analysis demonstrate that the computational complexity of our algorithm is lower than that of the ES method.**

***Index Terms*—Intelligent reconfigurable surface (IRS), matching theory, optimization, terahertz (THz).**

I. INTRODUCTION

THE exponential growth in the number of connected devices and multimedia applications have dramatically increased the demand for large bandwidth (BW) and high data rate transmissions [1]. To accommodate these demands, the possible use of the terahertz (THz) band has attracted great interest from both industry and academia. The THz band can provide large available BW (from 0.1 THz to 10 THz) and a higher data rate of up to 1 terabits-per-second (Tbps), compared with the millimeter-wave (mmWave) band [2], [3]. In our model, we aim to improve the network's sum rate. In this context, the THz band is considered to be a promising candidate to enable beyond fifth-generation (B5G) and sixth-generation (6G) wireless communications [4].

*M. Rahim and T. L. Nguyen are with the Department of Electrical Engineering, École de Technologie Supérieure (ÉTS), Université du Québec, Montréal, QC H3C 1K3, Canada (emails: muddasir.rahim.1@ens.etsmtl.ca, thanh-luan.nguyen.1@ens.etsmtl.ca,).

**G. Kaddoum is with Department of Electrial Engineering, École de Technologie Supérieure (ÉTS), Université du Québec, Montréal, QC H3C 1K3, Canada and Artificial Intelligence & Cyber Systems Research Center, Lebanese American University (email: georges.kaddoum@etsmtl.ca)

†T. N. Do is with the Department of Electrical Engineering, Polytechnique Montreal, QC H3T 1J4, Canada (email: tri-nhu.do@polymtl.ca).

The THz band has many advantages, but establishing a reliable transmission link at THz frequencies is not easy [5]. The reason is that there are strong atmospheric attenuations, extremely high free-space losses, and the line-of-sight (LOS) channel is highly sensitive to blockage effects. This may negatively affect the communication range and reduce service coverage of THz communication networks. In the context of THz communications, deploying ultra-massive multiple-input-multiple-output (MIMO) systems may provide significant signal gains and potentially overcome the mentioned problem, however, ultra-massive MIMO requires a huge power source [6].

Recently, intelligent reconfigurable surfaces (IRSs) have become a promising technology to tackle the above problem of THz networks [7]. IRSs are made of a massive number of small passive and metamaterial-based reconfigurable elements, and an IRS can manipulate both the phase and amplitude of incident signals to reflect the signals in the desired directions. In addition, IRSs can be utilized to improve the performance of wireless communication systems, including for coverage extension, confidentiality improvement, and fairness guarantee. Specifically, the use of IRSs is useful when the LOS channel is blocked or has weak received signal power since it is possible to provide additional transmission links by utilizing the reflecting elements of an IRS.

IRS can be considered as passive IRS or active IRS. In the case of passive IRS, no power is needed when it manipulates the incident signal with the fixed reflecting coefficients. However, some power-aided circuits are deployed at the IRS to adjust the PS of each IRS element, which can be tens of microwatts per reflecting element [8]. In the case of active IRS, each reflecting element is supported by an active load impedance. The active IRS is similar to an active reflector, which adjusts the PS as well as performs the power amplification, with a less complex and power-hunger radio frequency (RF) chain [9]. However, signal amplification at the active IRS also amplifies the received noise at the IRS, ultimately increasing the noise power at the receiver. Furthermore, the active IRS is suitable for space-limited cases where deploying massive reflecting elements is difficult [9]. Moreover, unlike other transmission technologies such as active relay [10] IRS-aided networks are cost-efficient and energy-efficient because the IRS does not need power amplifiers and is composed of passive reflecting elements. Based on the benefits of THz bands and IRSs, we introduce three potential application frameworks, namely, IRS-aided outdoor communications (i.e., dense building outdoor scenarios), IRS-aided indoor communications, and IRS-aided unmanned aerial vehicle (UAV) communications [11].

This work is licensed under a Creative Commons Attribution-NonCommercial-NoDerivatives 4.0 License. For more information, see https://creativecommons.org/licenses/by-nc-nd/4.0/

This article has been accepted for publication in IEEE Open Journal of the Communications Society. This is the author's version which has not been fully edited and content may change prior to final publication. Citation information: DOI 10.1109/OJCOMS.2024.3353173

Specifically, the IEEE 802.15.3d standard selected the frequency range of 0.252-0.325 THz to support applications that require tens of gigabits per second (Gbps) in data rate [3].

Compared to single IRS-aided wireless networks, multiple IRS-aided wireless networks were shown to be more robust and capable of providing a greater range of services [12]. However, IRSs may have limited computing capabilities to support signal processing, especially when heterogeneous IRS deployment in a given network area is considered. In such a scenario, user pairing is essential for maximizing the IRS's efficiency. In addition, to maximize the sum rate through multiple IRS-aided wireless networks, a fast and efficient IRS scheduling policy is vital. Due to the binary association variables, the IRS association problems are generally non-deterministic polynomial-time hard (NP-hard) in general, which necessitates proper algorithm design. Meanwhile, there are two potential approaches. One is to relax the binary variables to continuous ones and use the Lagrangian dual decomposition scheme, as in [13]. However, the relaxed variables may result in loose upper-bound solutions that are not sufficiently accurate for the original problems. The second approach is to treat the association problem as a matching game. Motivated by these facts, we propose a low-complexity matching-based IRS scheduling scheme, i.e., the scheduling from each transmitter to an IRS and from that particular IRS to a receiver, that maximizes the sum rate of the entire network.

A. Related Works

Existing works on IRS-aided networks mostly focus on the phase shift (PS) matrix with passive beamforming at the IRS to maximize the signal-to-noise ratio (SNR), sum rate, secrecy rate, or energy efficiency [14–17], without considering IRS selection. A distributed IRS-aided wireless network was proposed in [14] to maximize achievable sum rates by optimizing the PS matrix with passive beamforming at all distributed IRSs and the transmit power vector at the sources. Moreover, the use of multiple IRS-aided mmWave communications to maximize the secrecy rate has been investigated in [15] and proposed a joint optimization of IRS PSs, transmit beamforming, and IRS on-off status. In [16], the authors investigated the robust joint design of the IRS-assisted cell-free MIMO communication network, where the objective was to maximize the average sum rate by jointly designing the active transmit beamforming of the APs and passive reflecting beamforming of the IRS. The authors in [17] demonstrated the energy efficiency of IRS-aided cell-free MIMO networks. In this context, the authors proposed a hybrid beamforming technique consisting of digital beamforming at APs and analog beamforming on the IRS to maximize energy efficiency. The authors in [18] proposed a prioritized signal-enhancement-based (SEB) method, where passive beamforming is designed for the user with the best channel gain, and all the other users rely on IRS-enhanced beamforming.

There are few studies that addressed the problem of IRS-user scheduling in multiple-input-single-output (MISO) networks. The authors in [19] proposed IRS selection strategies for multi-IRS-aided wireless networks in which the number of elements of each IRS can be arbitrarily set. The performance analysis was carried out based on assuming that the magnitudes of the channel coefficients associated with different IRSs are independent and identically distributed (IID) random variables. In [20], the authors proposed an IRS selection policy that maximizes the end-to-end (e2e) SNR for multi-IRS-aided networks. In this context, the authors only consider the impact of pathloss (PL) and ignore channel fading effects. The effect of distributed and centralized IRS deployment schemes on the capacity region of multi-IRS-aided wireless networks has been demonstrated in [21]. According to the authors, in distributed IRS deployments, the channels associated with each distributed IRS are subject to IID Rayleigh fading.

TABLE I
COMPARISON OF RELATED WORK ON IRS-ASSISTED COMMUNICATIONS

Ref.	DN	MI	IA	PSC	THz	M	Performance metrics
[14]	✔	✔	✗	✔	✗	Small	Sum rate
[15]	✔	✔	✗	✔	✗	Small	Secrecy rate
[16]	✔	✔	✗	✔	✗	Small	Sum rate
[17]	✔	✔	✗	✔	✗	Small	Energy efficiency
[18]	✔	✔	✗	✔	✗	Small	Outage probability
[19]	✔	✔	✔	✗	✗	Small	Outage probability
[20]	✔	✔	✔	✗	✗	Large	Channel gain
[22]	✔	✔	✔	✗	✗	Large	Bit error rate
[23]	✔	✔	✔	✔	✗	Large	Sum rate
[24]	✔	✔	✔	✗	✗	Large	Average SINR
[25]	✔	✔	✔	✗	✗	Small	Average throughput
Proposed	✔	✔	✔	✔	✔	Very large	Sum rate

Distributed network (DN), multiple IRS (MI), IRS association (IA), PS configuration (PSC), Number of reflecting elements (M).

The authors in [22] considered multi-IRS-aided wireless networks for both outdoor and indoor communications, where the direct channel between a transmitter and a receiver is blocked. A low-complexity IRS selection scheme that uses the IRS with the highest SNR for communication is proposed in this study. However, small-scale fading was not considered, and no performance analysis was performed. In [23], the authors derived the asymptotic optimal solution for passive beamforming to maximize the achievable sum rate of the IRS-assisted network. Furthermore, this work proposed a joint user association and transmit power control in a multi-user downlink network to maximize the sum rate of the network. The authors in [24] formulated the optimization problem to maximize the minimum average signal-to-interference-plus-noise ratio (SINR) among all users by optimizing the IRS-user allocations. The nearest association (NA) method is proposed, where each user is associated with the IRS which is closest to it among all IRSs. In [25], the authors considered an IRS-aided cellular-based internet-of-things (IoT) system model where the IoT devices are powered by the ambient radio frequency (RF) energy from cellular transmissions. Moreover, the NA method is used for IoT devices to the APs association and for IoT devices to the IRSs association.

B. Contributions

In contrast to the aforementioned related works, this paper considers the Tx-IRS-Rx scheduling problem in IRS-aided networks

This work is licensed under a Creative Commons Attribution-NonCommercial-NoDerivatives 4.0 License. For more information, see https://creativecommons.org/licenses/by-nc-nd/4.0/

This article has been accepted for publication in IEEE Open Journal of the Communications Society. This is the author's version which has not been fully edited and content may change prior to final publication. Citation information: DOI 10.1109/OJCOMS.2024.3353173

as a matching problem. To the best of our knowledge, this is the first paper to study the Tx-IRS-Rx allocation problem in IRS-aided THz networks in the presence of imperfect channel state information (CSI) knowledge in order to improve the sum rate. A comparison of existing works on IRS-assisted communications and the novelty of the proposed work is summarized in Table I-A. The key contributions of this paper are summarized as follows:

- In this paper, we derive the channel model for IRS-aided THz networks without direct channels. We also propose a new angle-based trigonometric PL model and compare it to existing models to validate its correctness.
- In order to maximize the sum rate, we propose a method to formulate the allocation problem as a three-dimensional (3D) matching problem. Furthermore, we mathematically prove that the formulated problem is NP-hard. We then propose a global optimal solution for the formulated 3D allocation problem by leveraging the exhaustive search (ES) method as a benchmark.
- For the formulated association problem, we first decompose the 3D problem into two 2D sub-problems. We then propose two consecutive Gale-Shapley algorithms for the decomposed problems to obtain a sub-optimal solution to the original problem. Moreover, the proposed sub-optimal solution is near-optimal and significantly reduces the computational complexity.
- We prove that the proposed matching-based algorithm converges to a stable matching and terminates after a finite number of iterations.
- Numerical results demonstrate that the proposed matching-based allocation can significantly improve the sum rate compared to the NA, greedy search (GS), and random assignment (RA). Additionally, the sum rate of the proposed method is compatible with the sum rate of the ES method, while the computational complexity of the proposed method is lower than the ES method.

C. Paper Organization and Notation

The remainder of the paper is outlined as follows. First, the system model, including the IRS PS configurations, channel modeling, and the SINR formulation, is illustrated in Section II. The IRS association optimization problem is formulated in Section III. In Section IV, an optimal solution is provided, and the proposed low-complexity algorithm is presented in Section V. The performance of the proposed approach is examined in Section VI, and the paper is concluded in Section VII.

Notations: Boldface lowercase and uppercase symbols are used for vectors and matrices, respectively. The symbols $\mathbf{X}^{\mathsf{T}}$ and $\mathbf{X}^{\mathsf{H}}$ denote the transpose and conjugate transpose (Hermitian) of matrix $\mathbf{X}$, respectively. We use $[\mathbf{x}]_n$ and $[\mathbf{X}]_{n,m}$ to represent the n-th and (n,m)-th elements of the respective vector $\mathbf{x}$ and matrix $\mathbf{X}$, respectively. The notations $|.|$ and $\|.\|$ are the absolute value and L2-norm operators, respectively. $\mathbb{E}[.]$ denotes the statistical expectation. $\mathbb{R}^{M\times 1}$ and $\mathbb{C}^{M\times 1}$ denote the set of real and complex vectors of length $M\times 1$, respectively. We use $\mathcal{CN}(\mu,\sigma^2)$ to define a circularly symmetric complex Gaussian (CSCG) random variable with mean μ and variance σ^2. Finally, $\mathbf{X}^\star$ and $\overline{\mathbf{X}}$ denote the optimal and near-optimal values of the optimization variable $\mathbf{X}$, respectively. Important system parameters and channel variables used in this paper are detailed in Table I-C.

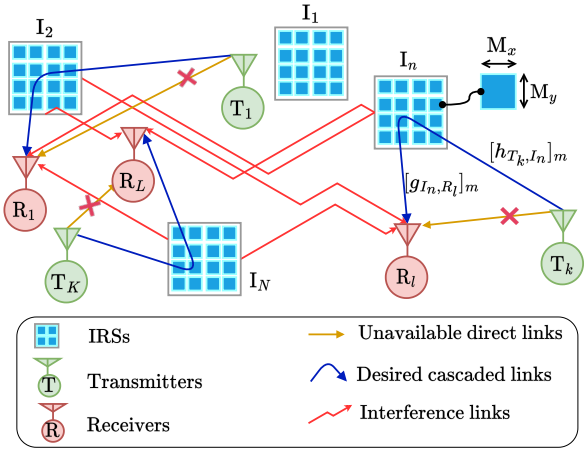


Fig. 1. IRS-aided networks over THz band.

II. System Model

We consider IRS-aided networks using THz bands where the IRSs are used to assist the communication between the transmitter (Tx) and the receiver (Rx). The network consists of a set of available Txs $\mathcal{T}=\{\mathrm{T}_1,\mathrm{T}_2,\ldots,\mathrm{T}_K\}$ and a set of distributed Rxs $\mathrm{R}=\{\mathrm{R}_1,\mathrm{R}_2,\ldots,\mathrm{R}_L\}$, with a cardinality of K and L, respectively. The locations of the nodes are assumed to be random but uniformly distributed within a defined region. Furthermore, we assume that the reflecting elements are passive and that no power is needed when it reflects the incident signal[1] [9]. The set of N available distributed IRSs is denoted as $\mathcal{I}=\{\mathrm{I}_1,\mathrm{I}_2,\ldots,\mathrm{I}_N\}$, where the n^{th} IRS is equipped with M_n reflecting elements. The area of each IRS element is $A=M_x\times M_y$, where M_x and M_y denote the length of the horizontal and vertical sides, respectively. Henceforth, we use T, R, and I as acronyms for the Tx, Rx, and IRS, respectively. In addition, we assume all direct links are blocked[2] due to severe shadowing by obstacles or human bodies in the environment [4], [26], and receivers are served through IRS cascaded links, as shown in Fig. 1. Through a well-planned deployment of the IRSs, we consider that there exists a LOS path between the T-to-I link and the I-to-R link. In THz channels, the pathloss of the non-LOS (NLOS) links is known to be much larger than that of the LOS links due to smaller wavelengths [27]. Therefore, we ignore the NLOS links between the T-to-I link and

[1]The consideration of passive reflecting elements is suitable when we deploy a large number of reflecting elements at THz bands while active IRS is suitable for a small number of reflecting elements [9]. Moreover, some switch circuits are used at passive IRS, enabling each reflecting element to reconfigure its reflection coefficient, which requires minimal power, i.e., tens of microwatt per reflecting element [8].

[2]This assumption is reasonable when the direct link is severely obstructed by obstacles or human bodies in the environment [4], [26].

This work is licensed under a Creative Commons Attribution-NonCommercial-NoDerivatives 4.0 License. For more information, see https://creativecommons.org/licenses/by-nc-nd/4.0/

This article has been accepted for publication in IEEE Open Journal of the Communications Society. This is the author's version which has not been fully edited and content may change prior to final publication. Citation information: DOI 10.1109/OJCOMS.2024.3353173

TABLE II
LIST OF MATHEMATICAL NOTATIONS

Notation	Description
K	Number of transmitters.
L	Number of receivers.
N	Number of IRSs.
M	Number of IRS reflecting elements.
T_k	k^{th} transmitter.
R_l	l^{th} receiver.
I_n	n^{th} IRS.
$\mathrm{I}_{n,m}$	m^{th} reflecting element on I_n.
$\mathbf{c}_{\mathrm{I}}^{n}$	Center location of I_n.
$\mathbf{c}_{\mathrm{T}}^{k}$	Center location of T_k.
$\mathbf{c}_{\mathrm{R}}^{l}$	Center location of R_l.
$d_{\mathrm{T}_k,\mathrm{I}_n}$	Distance between T_k to I_n.
$d_{\mathrm{I}_n,\mathrm{R}_l}$	Distance between I_n to R_l.
ψ	Evaluation angle.
ϕ	Azimuth angle.
x_k	Transmit signal of transmitter k.
$\widehat{\mathbf{h}}_{\mathrm{T}_k,\mathrm{I}_n} \in \mathbb{C}^{M\times 1}$	EC vector from T_k-to-I_n.
$\widetilde{\mathbf{h}}_{\mathrm{T}_k,\mathrm{I}_n}$	CEErs from T_k-to-I_n.
$\mathbf{h}_{\mathrm{T}_k,\mathrm{I}_n} \in \mathbb{C}^{M\times 1}$	Channel vector from T_k-to-I_n.
$\widehat{\mathbf{g}}_{\mathrm{I}_n,\mathrm{R}_l} \in \mathbb{C}^{M\times 1}$	EC vector from I_n-to-R_l.
$\widetilde{\mathbf{g}}_{\mathrm{I}_n,\mathrm{R}_l}$	CEEs from I_n-to-R_l.
$\mathbf{g}_{\mathrm{I}_n,\mathrm{R}_l} \in \mathbb{C}^{M\times 1}$	Channel vector from I_n-to-R_l.
$h_{\mathrm{T}_k,\mathrm{I}_n,\mathrm{R}_l}$	Cascaded channel from T_k-to-R_l through I_n.
$\widehat{h}_{\mathrm{T}_k,\mathrm{I}_n,\mathrm{R}_l}$	Cascaded EC from T_k-to-R_l through I_n.
$\widetilde{h}_{\mathrm{T}_k,\mathrm{I}_n,\mathrm{R}_l}$	CEE from T_k-to-R_l through I_n.
$\xi_{\mathrm{T}_k,\mathrm{I}_{n,m}}$	Pathloss in $\mathrm{T}_k \to \mathrm{I}_{n,m}$ link.
$\xi_{\mathrm{I}_{n,m},\mathrm{R}_l}$	Pathloss in $\mathrm{I}_{n,m} \to \mathrm{R}_l$ link.
$\xi_{\mathrm{T}_k\mathrm{I}_{n,m},\mathrm{R}_l}$	Pathloss in $\mathrm{T}_k \to \mathrm{I}_{n,m} \to \mathrm{R}_l$ link.
$\boldsymbol{\Theta}_n$	IRS reflection matrix.
$\kappa_{n,m} \in (0,1]$	Reflection coefficient of $\mathrm{I}_{n,m}$.
$\theta_{n,m} \in [0, 2\pi)$	Phase shift applied by $\mathrm{I}_{n,m}$.
p_k	Transmit power of R_k.
$\mathbf{r}_{k,n,m}$	Incident direction from T_k-to-$\mathrm{I}_{n,m}$.
$\mathbf{r}_{n,m,l}$	Reflection direction from $\mathrm{I}_{n,m}$-to-R_l.
$\mathbb{G}_{\mathrm{I}_{n,m}}(-\mathbf{r}_{k,n,m})$	Gains of $\mathrm{I}_{n,m}$ in the incident direction $\mathbf{r}_{n,m,l}$.
$\mathbb{G}_{\mathrm{I}_{n,m}}(\mathbf{r}_{n,m,l})$	Gains of $\mathrm{I}_{n,m}$ in the reflection direction $\mathbf{r}_{n,m,l}$.
$\mathbb{G}_{\mathrm{T}_k}$	Antenna gain at T_k.
$\mathbb{G}_{\mathrm{R}_l}$	Antenna gain at R_l.
$y_{\mathrm{T}_k,\mathrm{I}_n,\mathrm{R}_l}$	Received signal at R_l from T_k through I_n.
$[\boldsymbol{\Omega}]^{\star}_{\mathrm{T}_k,\mathrm{I}_n,\mathrm{R}_l}$	Allocation matrix obtained with ES method.
$[\widehat{\boldsymbol{\Omega}}]_{\mathrm{T}_k,\mathrm{I}_n,\mathrm{R}_l}$	Allocation matrix obtained with proposed algorithm.
$\mathrm{SINR}_{\mathrm{T}_k,\mathrm{I}_n,\mathrm{R}_l}$	SINR from $\mathrm{T}_k \to \mathrm{I}_n \to \mathrm{R}_l$ link.
$R_{\mathrm{T}_k,\mathrm{I}_n,\mathrm{R}_l}$	Data rate of $\mathrm{T}_k \to \mathrm{I}_n \to \mathrm{R}_l$ link.
$\Xi_{\mathrm{T}_k,\mathrm{I}_n,:}$	Pseudo SINRs from $\mathrm{T}_k \to \mathrm{I}_n$ link.
$\Xi_{\mathrm{T}_{k^\star},\mathrm{I}_{n^\star},\mathrm{R}_l}$	Pseudo SINRs from $\mathrm{T}_{k^\star} \to \mathrm{I}_{n^\star} \to \mathrm{R}_l$ link.
$\Lambda_{\mathrm{T}_k,\mathrm{I}_n,:}$	Pseudo data rate of $\mathrm{T}_k \to \mathrm{I}_n$ link.
$\Lambda_{\mathrm{T}_{k^\star},\mathrm{I}_{n^\star},\mathrm{R}_l}$	Pseudo data rate of $\mathrm{T}_{k^\star} \to \mathrm{I}_{n^\star} \to \mathrm{R}_l$ link.

the I-to-R link. Furthermore, we only consider signals reflected by an IRS one time because the signals reflected by the IRS two times or more are weak and can be neglected [28].

A. 3D Cartesian Coordinates (x, y, z)

In the Cartesian coordinate system, the center locations of the n^{th} IRS (I_n), the k^{th} T (T_k), and the l^{th} R (R_l) are defined as $\mathbf{c}_{\mathrm{I}}^{n} = (x_{\mathrm{I}}^{n}, y_{\mathrm{I}}^{n}, z_{\mathrm{I}}^{n})$, $\mathbf{c}_{\mathrm{T}}^{k} = (x_{\mathrm{T}}^{k}, y_{\mathrm{T}}^{k}, z_{\mathrm{T}}^{k})$, and $\mathbf{c}_{\mathrm{R}}^{l} = (x_{\mathrm{R}}^{l}, y_{\mathrm{R}}^{l}, z_{\mathrm{R}}^{l})$, respectively. The vectors joining T_k to the m^{th} reflecting element on I_n ($\mathrm{I}_{n,m}$) and $\mathrm{I}_{n,m}$-to-R_l are expressed as $\mathbf{r}_{k,n,m} = (x_{\mathrm{T}}^{k} - x_{\mathrm{I}}^{n,m}, y_{\mathrm{T}}^{k} - y_{\mathrm{I}}^{n,m}, z_{\mathrm{T}}^{k} - z_{\mathrm{I}}^{n,m})$, and $\mathbf{r}_{n,m,l} = (x_{\mathrm{R}}^{k} - x_{\mathrm{I}}^{n,m}, y_{\mathrm{R}}^{k} - y_{\mathrm{I}}^{n,m}, z_{\mathrm{R}}^{k} - z_{\mathrm{I}}^{n,m})$, respectively.

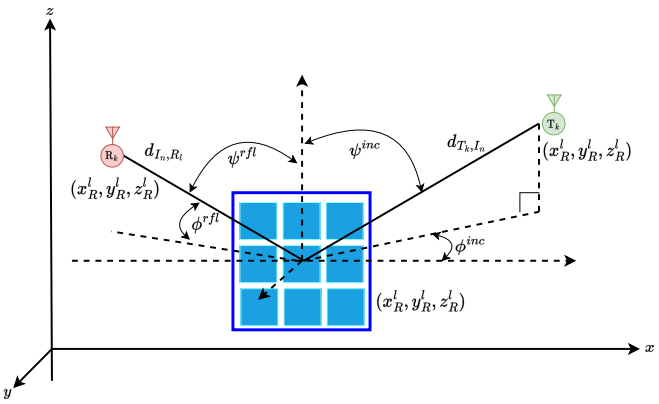


Fig. 2. Illustration of 3D geometry of the IRS-aided network considered in the channel model.

B. 3D Cartesian to Spherical Coordinates (d, ψ, ϕ)

The Cartesian coordinates (x, y, z) of a node's location can be converted into spherical coordinates (d, ψ, ϕ), where d, ψ, and ϕ represent the distance, elevation angle, and azimuth angle, respectively. Let $d_{\mathrm{T}_k,\mathrm{I}_{n,m}}$ denote the distance from T_k to $\mathrm{I}_{n,m}$, and $d_{\mathrm{I}_{n,m},\mathrm{R}_l}$ denote the distance from $\mathrm{I}_{n,m}$ to R_l, as shown in Fig. 2. For THz communications, the elements of the IRS are densely installed, and we ignore the distance between the IRS elements. Thus, the distances $d_{\mathrm{T}_k,\mathrm{I}_n}$ and $d_{\mathrm{I}_n,\mathrm{R}_l}$ can be computed from the center location of I_n to T_k and R_l, respectively, which are expressed as

$$d_{\mathrm{T}_k,\mathrm{I}_n} = \sqrt{(x_{\mathrm{T}}^{k} - x_{\mathrm{I}}^{n})^2 + (y_{\mathrm{T}}^{k} - y_{\mathrm{I}}^{n})^2 + (z_{\mathrm{T}}^{k} - z_{\mathrm{I}}^{n})^2}, \quad (1)$$

$$d_{\mathrm{I}_n,\mathrm{R}_l} = \sqrt{(x_{\mathrm{R}}^{k} - x_{\mathrm{I}}^{n})^2 + (y_{\mathrm{R}}^{k} - y_{\mathrm{I}}^{n})^2 + (z_{\mathrm{R}}^{k} - z_{\mathrm{I}}^{n})^2}. \quad (2)$$

Elevation Angle: In order to determine the height of the node, the angle between the z-axis and the radius is measured, known as the elevation angle. The unit vectors in the direction of the x-axis, y-axis, and z-axis are given by $\mathbf{r}_x = (1, 0, 0)$, $\mathbf{r}_y = (0, 1, 0)$, and $\mathbf{r}_z = (0, 0, 1)$, respectively. The cosine of $\psi_{k,n,m}^{\mathrm{inc}}$ is obtained as

$$\cos\left(\psi_{k,n,m}^{\mathrm{inc}}\right) = \left[\frac{\mathbf{r}_{k,n,m}\mathbf{r}_z}{\|\mathbf{r}_{k,n,m}\| \, \|\mathbf{r}_z\|}\right] = \left[\frac{z_{\mathrm{T}}^{k} - z_{\mathrm{I}}^{n,m}}{d_{\mathrm{T}_k,\mathrm{I}_{n,m}}}\right]. \quad (3)$$

As a result, the cosine of $\psi_{n,m,l}^{\mathrm{rfl}}$ from $\mathrm{I}_{n,m}$ to R_l is calculated as

$$\cos\left(\psi_{n,m,l}^{\mathrm{rfl}}\right) = \left[\frac{z_{\mathrm{R}}^{l} - z_{\mathrm{I}}^{n,m}}{d_{\mathrm{I}_{n,m},\mathrm{R}_l}}\right]. \quad (4)$$

Azimuth Angle: The azimuth angle is measured in relation to the x-axis and to the radius projected into the 2D plane, which determines the direction of the node. The tangent of $\phi_{k,n,m}^{\mathrm{inc}}$ can be written as

$$\tan\left(\phi_{k,n,m}^{\mathrm{inc}}\right) = \left[\frac{\mathbf{r}_{k,n,m}\mathbf{r}_y}{\mathbf{r}_{k,n,m}\mathbf{r}_x}\right] = \left[\frac{y_{\mathrm{T}}^{k} - y_{\mathrm{I}}^{n,m}}{x_{\mathrm{T}}^{k} - x_{\mathrm{I}}^{n,m}}\right]. \quad (5)$$

As a result, the tangent of $\phi_{n,m,l}^{\mathrm{rfl}}$ from $\mathrm{I}_{n,m}$ to R_l is obtained as

$$\tan\left(\phi_{n,m,l}^{\mathrm{rfl}}\right) = \left[\frac{y_{\mathrm{R}}^{l} - y_{\mathrm{I}}^{n,m}}{x_{\mathrm{R}}^{l} - x_{\mathrm{I}}^{n,m}}\right]. \quad (6)$$

This work is licensed under a Creative Commons Attribution-NonCommercial-NoDerivatives 4.0 License. For more information, see https://creativecommons.org/licenses/by-nc-nd/4.0/

This article has been accepted for publication in IEEE Open Journal of the Communications Society. This is the author's version which has not been fully edited and content may change prior to final publication. Citation information: DOI 10.1109/OJCOMS.2024.3353173

C. IRS Phase-Shift Configurations

Introducing a PS to impinging signals is an important characteristic of the IRS. The PS matrix combines the amplitude and PS of each element of the IRS. The PS matrix of the I_n can be described as [29]:

$$\mathbf{\Theta}_n = \mathrm{diag}([\kappa_{n,1}e^{j\theta_{n,1}}, ..., \kappa_{n,m}e^{j\theta_{n,m}}, ..., \kappa_{n,M}e^{j\theta_{n,M}}]), \quad (7)$$

where $\kappa_{n,m} \in (0, 1]$ and $\theta_{n,m} \in [0, 2\pi)$ represent the amplitude and the PS of $\mathrm{I}_{n,m}$, respectively. The PS matrix can be categorized into three categories depending on the deployment of the IRS [30], namely (i) continuous amplitude and PS, where the amplitude and PS of the IRS elements are continuously adjusting, (ii) constant amplitude and continuous PS, where the amplitude is constant, e.g., $\kappa_{n,m} = 1$, and the PS can be continuously adjusted, and (iii) constant amplitude and discrete PS, where the amplitude is fixed and the PS is adjusted based on a discrete set of values.

D. Channel Modeling of the Considered IRS-THz System

Assuming that T_k transmits a signal x_k with transmission power p_k, where $\mathbb{E}[|x_k|^2] = 1$. We assume that the direct link between the T and the R is blocked by an obstacle, and therefore focus on the propagation model for cascaded links. Additionally, we consider that the CSI available at the transmitters, receivers, and IRSs is imperfect[3].

The wireless channel can be achieved by either the near-field or far-field models. The communications in the near-field regions are spherical-wave-based, while planar-wave-based in the far-field regions. To differentiate the near-field or far-field regions, we define the Rayleigh distance d_{ray} as a boundary, which can be expressed as [34]

$$d_{ray} = \frac{2D^2}{\lambda}. \quad (8)$$

where D is the aperture of the IRS. Moreover, the range of near-field region can be expressed as [34]

$$d_{\mathrm{T}_k,\mathrm{I}_n} < d_{ray}, \quad d_{\mathrm{I}_n,\mathrm{R}_l} < d_{ray}. \quad (9)$$

The range after the near-field region in (9) is considered as the far-field region, and the communication in this region is far-field communication. For the carrier frequency $f_c = 300$ GHz, $\lambda = 0.001\,m$, and side length of IRS elements 0.4λ [35], we calculate the Rayleigh distance d_{ray} for different numbers of IRS elements as shown in Table III. From Table III, we verify that the Rayleigh distance d_{ray} is very small which makes the range of near-field communication is very limited. Thus we ignore this region and consider the far-field communication.

[3]Channel estimation is much more difficult in IRS-assisted wireless communication than in traditional wireless networks. Furthermore, it is more challenging at the IRS than the Tx / Rx because the IRS has passive reflecting elements that cannot process the pilot signals sent from and to the Tx / Rx [31], [32]. However, channel reciprocity holds for the Tx-to-IRS and IRS-to-Rx channels [33]. We, therefore, assume that the estimated CSI at the Tx / Rx is similar to the IRS's CSI.

TABLE III
RAYLEIGH DISTANCE d_{ray} WITH VARYING NUMBER OF IRS ELEMENTS.

$M = M_x \times M_y$	Physical size of IRS $[m^2]$	$d_{ray}\,[m]$
30×30	0.012×0.012	0.288
50×50	0.02×0.02	0.8
100×100	0.04×0.04	3.2

1) Tx to IRS Channel Modeling: Let $\widehat{\mathbf{h}}_{\mathrm{T}_k,\mathrm{I}_n} \in \mathbb{C}^{M\times 1}$ denote the estimated channel (EC) vector from T_k-to-I_n. In this context, $[\widehat{\mathbf{h}}_{\mathrm{T}_k,\mathrm{I}_n}]_m = \widehat{h}_{\mathrm{T}_k,\mathrm{I}_{n,m}}$ is the individual channel from T_k-to-$\mathrm{I}_{n,m}$ which can be expressed as [36]

$$[\widehat{\mathbf{h}}_{\mathrm{T}_k,\mathrm{I}_n}]_m = \widehat{h}_{\mathrm{T}_k,\mathrm{I}_{n,m}} = \sqrt{\xi_{\mathrm{T}_k,\mathrm{I}_{n,m}}}e^{-j\frac{2\pi}{\lambda}d_{\mathrm{T}_k,\mathrm{I}_{n,m}}}, \quad (10)$$

where $\frac{2\pi}{\lambda}$ is the wavenumber and $\xi_{\mathrm{T}_k,\mathrm{I}_{n,m}}$ represents the PL of the T_k-to-$\mathrm{I}_{n,m}$ link which can be expressed as [37], [38]

$$\xi_{\mathrm{T}_k,\mathrm{I}_{n,m}} = \mathbb{G}_{\mathrm{T}_k}\mathbb{G}_{\mathrm{I}_{n,m}}(-\mathbf{r}_{k,n,m})\frac{A^2e^{-\kappa_{abs}(f)d_{\mathrm{T}_k,\mathrm{I}_{n,m}}}}{(4\pi d_{\mathrm{T}_k,\mathrm{I}_{n,m}})^2}, \quad (11)$$

where $\kappa_{abs}(f)$ is the absorption coefficient at the carrier frequency f, $\mathbb{G}_{\mathrm{T}_k}$ is antenna gain at T_k, and $\mathbb{G}_{\mathrm{I}_{n,m}}(-\mathbf{r}_{k,n,m})$ denotes the gains of $\mathrm{I}_{n,m}$ in the incident direction, which can be written as [39]

$$\mathbf{r}_{k,n,m} = d_{\mathrm{T}_k,\mathrm{I}_{n,m}}\begin{pmatrix}\cos(\psi^{\mathrm{inc}}_{k,n,m})\cos(\phi^{\mathrm{inc}}_{k,n,m})\\ \cos(\psi^{\mathrm{inc}}_{k,n,m})\sin(\phi^{\mathrm{inc}}_{k,n,m})\\ \sin(\psi^{\mathrm{inc}}_{k,n,m})\end{pmatrix}, \quad (12)$$

where ψ and ϕ are the elevation and azimuth angles from the IRS unit to a certain transmitting/receiving direction. Furthermore, the actual channel with the CSI estimation errors (CEEs) can be expressed as

$$\mathbf{h}_{\mathrm{T}_k,\mathrm{I}_n} = \widehat{\mathbf{h}}_{\mathrm{T}_k,\mathrm{I}_n} + \widetilde{\mathbf{h}}_{\mathrm{T}_k,\mathrm{I}_n}, \quad (13)$$

where $\widetilde{\mathbf{h}}_{\mathrm{T}_k,\mathrm{I}_n}$ denotes the CEEs, which are uncorrelated with the estimated channel $\widehat{\mathbf{h}}_{\mathrm{T}_k,\mathrm{I}_n}$, and the entries of $\widetilde{\mathbf{h}}_{\mathrm{T}_k,\mathrm{I}_n}$ are IID complex Gaussian with zero mean and variance $\sigma^2_{\mathbf{g}_{\mathrm{T}_k,\mathrm{I}_n}}$.

2) IRS to Rx Channel Modeling: The received power $p_n = p_k\xi_{\mathrm{T}_k,\mathrm{I}_{n,m}}$ at I_n from T_k can be calculated using the PL in (11). Let $\widehat{\mathbf{g}}_{\mathrm{I}_n,\mathrm{R}_l} \in \mathbb{C}^{M\times 1}$ denotes the EC gain vector of the I_n-to-R_l links, and $[\widehat{\mathbf{g}}_{\mathrm{I}_n,\mathrm{R}_l}]_m = \widehat{g}_{\mathrm{I}_{n,m},\mathrm{R}_l}$ be the individual channel from $\mathrm{I}_{n,m}$-to-R_l, which can be expressed as [36]

$$[\mathbf{g}_{\mathrm{I}_n,\mathrm{R}_l}]_m = g_{\mathrm{I}_{n,m},\mathrm{R}_l} = \sqrt{\xi_{\mathrm{I}_{n,m},\mathrm{R}_l}}e^{-j\frac{2\pi}{\lambda}d_{\mathrm{I}_{n,m},\mathrm{R}_l}}, \quad (14)$$

where $\xi_{\mathrm{I}_{n,m},\mathrm{R}_l}$ represents the PL of the $\mathrm{I}_{n,m}$-to-R_l link which can be expressed as

$$\xi_{\mathrm{I}_{n,m},\mathrm{R}_l} = \mathbb{G}_{\mathrm{I}_{n,m}}(\mathbf{r}_{n,m,l})\mathbb{G}_{\mathrm{R}_l}\frac{A^2e^{-\kappa_{abs}(f)d_{\mathrm{I}_{n,m},\mathrm{R}_l}}}{(4\pi d_{\mathrm{I}_{n,m},\mathrm{R}_l})^2}, \quad (15)$$

where $\mathbb{G}_{\mathrm{R}_l}$ is antenna gain at R_l and $\mathbb{G}_{\mathrm{I}_{n,m}}(\mathbf{r}_{n,m,l})$ are the gains of $\mathrm{I}_{n,m}$ in the reflection direction $\mathbf{r}_{n,m,l}$, which can be written as [39]

$$\mathbf{r}_{n,m,l} = d_{\mathrm{I}_{n,m},\mathrm{R}_l}\begin{pmatrix}\cos(\psi^{\mathrm{rfl}}_{n,m,l})\cos(\phi^{\mathrm{rfl}}_{n,m,l})\\ \cos(\psi^{\mathrm{rfl}}_{n,m,l})\sin(\phi^{\mathrm{rfl}}_{n,m,l})\\ \sin(\psi^{\mathrm{rfl}}_{n,m,l})\end{pmatrix}. \quad (16)$$

This work is licensed under a Creative Commons Attribution-NonCommercial-NoDerivatives 4.0 License. For more information, see https://creativecommons.org/licenses/by-nc-nd/4.0/

This article has been accepted for publication in IEEE Open Journal of the Communications Society. This is the author's version which has not been fully edited and content may change prior to final publication. Citation information: DOI 10.1109/OJCOMS.2024.3353173

Meanwhile, the channel with CEEs $\widetilde{\mathbf{g}}_{\mathrm{I}_n,\mathrm{R}_l} \sim \mathcal{CN}(\mathbf{0}, \sigma^2_{\widetilde{\mathbf{g}}_{\mathrm{I}_n,\mathrm{R}_l}})$ can be expressed as

$$\mathbf{g}_{\mathrm{I}_n,\mathrm{R}_l} = \widehat{\mathbf{g}}_{\mathrm{I}_n,\mathrm{R}_l} + \widetilde{\mathbf{g}}_{\mathrm{I}_n,\mathrm{R}_l}. \tag{17}$$

The reflecting elements of the IRS can be designed to be identical in size and gain, with small size and low gain in the THz band. Therefore, the reflecting elements can have the same normalized power radiation pattern model given as [40]

$$\mathbb{U}_{\mathrm{I}_{n,m}}(\psi) = \cos^q(\psi), \quad 0 \leq \psi < \pi/2, \tag{18}$$

where q determines the directivity of each reflecting element. the above pattern solely relies on the elevation angle ψ, where the maximum antenna gain towards the IRS can be obtained with zero elevation angle, i.e., $\psi = 0$ [41]. Furthermore, the directivity of the reflecting element is also a function of the elevation angle ψ and is given as

$$\mathbb{D}_{\mathrm{I}_{n,m}}(\psi) = 2(q+1)\cos^q(\psi), \quad 0 \leq \psi < \pi/2. \tag{19}$$

The reflecting element's directivity is governed by the value of q in this model. In addition, the pattern in (18) is a cosine function raised to the power q, and as the value of q increases, the beam becomes more directive. Thus the gain of $\mathrm{I}_{n,m}$ can be expressed as

$$\mathbb{G}_{\mathrm{I}_n}(\psi,\phi) = \begin{cases} 2\gamma(q+1)\cos^q(\psi), & 0 \leq \psi < \pi/2, \\ 0, & \pi/2 \leq \psi \leq \pi, \end{cases} \tag{20}$$

where $\phi \in [0, 2\pi)$ and γ is the antenna efficiency of the IRS reflecting elements. Thus, the existing model is only applicable for a specific value of q and zero elevation angle, i.e., $\psi = 0$. Therefore, based on the existing PL models for THz frequencies [36], [37], we propose a new PL model that facilitates our network analysis.

3) Cascaded Channel Modeling: IRS elements scatter the incident wave in all directions rather than reflecting it with the same beam curvature. Therefore, some signals can be lost, which causes extra PL[4]. In the case of IRS-aided networks, the received signal power depends on the area and effective aperture of the IRS. When the IRS elements become infinitely large, they act as perfect mirrors that reflect all the incident waves according to Snell's reflection law [43]. Let $h_{\mathrm{T}_k,\mathrm{I}_n,\mathrm{R}_l}$ be the cascaded channel from T_k-to-R_l through I_n, which can be expressed as

$$\begin{aligned} h_{\mathrm{T}_k,\mathrm{I}_n,\mathrm{R}_l} &= (\mathbf{h}_{\mathrm{T}_k,\mathrm{I}_n})^T \boldsymbol{\Theta}_n \mathbf{g}_{\mathrm{I}_n,\mathrm{R}_l} \\ &= (\widehat{\mathbf{h}}_{\mathrm{T}_k,\mathrm{I}_n} + \widetilde{\mathbf{h}}_{\mathrm{T}_k,\mathrm{I}_n})^T \boldsymbol{\Theta}_n (\widehat{\mathbf{g}}_{\mathrm{I}_n,\mathrm{R}_l} + \widetilde{\mathbf{g}}_{\mathrm{I}_n,\mathrm{R}_l}) \\ &= \underbrace{\widehat{\mathbf{h}}^T_{\mathrm{T}_k,\mathrm{I}_n} \boldsymbol{\Theta}_n \widehat{\mathbf{g}}_{\mathrm{I}_n,\mathrm{R}_l}}_{\widehat{h}_{\mathrm{T}_k,\mathrm{I}_n,\mathrm{R}_l}} \\ &+ \underbrace{\widetilde{\mathbf{h}}^T_{\mathrm{T}_k,\mathrm{I}_n} \boldsymbol{\Theta}_n \widehat{\mathbf{g}}_{\mathrm{I}_n,\mathrm{R}_l} + \widehat{\mathbf{h}}^T_{\mathrm{R}_k,\mathrm{I}_n} \boldsymbol{\Theta}_n \widetilde{\mathbf{g}}_{\mathrm{I}_n,\mathrm{R}_l} + \widetilde{\mathbf{h}}^T_{\mathrm{T}_k,\mathrm{I}_n} \boldsymbol{\Theta}_n \widetilde{\mathbf{g}}_{\mathrm{I}_n,\mathrm{R}_l}}_{\widetilde{h}_{\mathrm{T}_k,\mathrm{I}_n,\mathrm{R}_l}}, \end{aligned} \tag{21}$$

[4]The amplitude of the IRS elements $\kappa_{n,m} \in (0,1]$, when the amplitude of the IRS element is less than 1, it means that the IRS is not fully reflecting the incident signal's power. In other words, some of the signal power is lost when it interacts with the IRS. Therefore, we set $\kappa_{n,m} = 1$ to avoid the extra PL [25], [42].

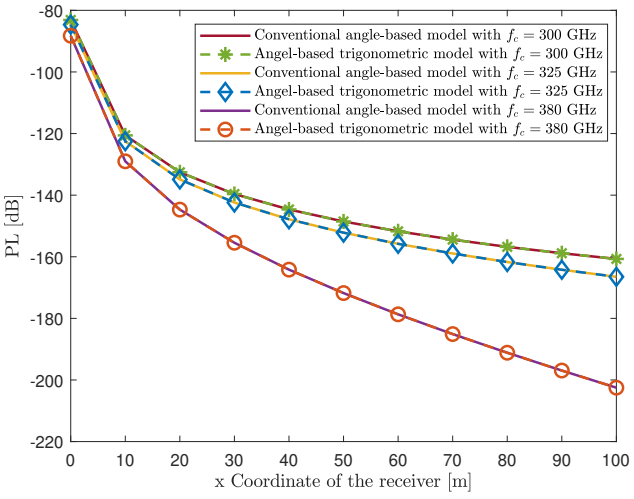


Fig. 3. Comparison between the conventional angel-based and the proposed angel-based trigonometric PL models for different frequencies.

where $\widetilde{h}_{\mathrm{T}_k,\mathrm{I}_n,\mathrm{R}_l}$ represents the CEEs, which is modeled as $\mathcal{CN}(\mathbf{0}, \sigma^2_{\widetilde{g}_{\mathrm{I}_n,\mathrm{R}_l}} |\widehat{\mathbf{h}}^T_{\mathrm{T}_k,\mathrm{I}_n} \widehat{\mathbf{h}}_{\mathrm{T}_k,\mathrm{I}_n}| + \sigma^2_{\widetilde{h}_{\mathrm{T}_k,\mathrm{I}_n}} |\widehat{\mathbf{g}}^T_{\mathrm{I}_n,\mathrm{R}_l} \widehat{\mathbf{g}}_{\mathrm{I}_n,\mathrm{R}_l}| + \sigma^2_{\widetilde{h}_{\mathrm{T}_k,\mathrm{I}_n}} \sigma^2_{\widetilde{g}_{\mathrm{I}_n,\mathrm{R}_l}})$.

Lemma 1. *Denoting* $\mathbb{G}_{\mathrm{I}_{n,m}}(\mathbf{r}^{\mathrm{inc}}, \mathbf{r}^{\mathrm{rfl}}) \triangleq \mathbb{G}_{\mathrm{I}_{n,m}}(-\mathbf{r}^{\mathrm{inc}}) \mathbb{G}_{\mathrm{I}_{n,m}}(\mathbf{r}^{\mathrm{rfl}})$ *as the cascaded gain of the* m^{th} *element of* I_n*, the angle-based trigonometric model of* $\mathbb{G}_{\mathrm{I}_{n,m}}(\mathbf{r}^{\mathrm{inc}}, \mathbf{r}^{\mathrm{rfl}})$ *is formulated as*

$$\mathbb{G}_{\mathrm{I}_{n,m}}(\mathbf{r}^{\mathrm{inc}}, \mathbf{r}^{\mathrm{rfl}}) = \left(\frac{4\pi A}{\lambda^2} \eta_{\mathrm{I}_{n,m}}(-\mathbf{r}^{\mathrm{inc}}, \mathbf{r}^{\mathrm{rfl}}) \right)^2, \tag{22}$$

$$\eta_{\mathrm{I}_{n,m}}(-\mathbf{r}^{\mathrm{inc}}, \mathbf{r}^{\mathrm{rfl}}) \triangleq \sqrt{\cos^2\psi^{\mathrm{inc}} (\cos^2\phi^{\mathrm{rfl}} \cos^2\psi^{\mathrm{rfl}} + \sin^2\phi^{\mathrm{rfl}})}.$$

Proof: The proof is provided in Appendix A. ■

Invoking Lemma 1, the PL of the cascaded link is the combination of the PLs over the T_k-to-I_n and I_n-to-R_l links, which can be expressed as

$$\begin{aligned} \xi_{\mathrm{T}_k,\mathrm{I}_n,\mathrm{R}_l} &= \mathbb{G}_{\mathrm{T}_k} \mathbb{G}_{\mathrm{I}_{n,m}}(-\mathbf{r}_{k,n,m}) \mathbb{G}_{\mathrm{I}_{n,m}}(\mathbf{r}_{n,m,l}) \mathbb{G}_{\mathrm{R}_l} \\ &\times \frac{\lambda^4 e^{-\kappa_{abs}(f)(d_{\mathrm{T}_k,\mathrm{I}_{n,m}} + d_{\mathrm{I}_{n,m},\mathrm{R}_l})}}{(4\pi)^4 (d_{\mathrm{T}_k,\mathrm{I}_{n,m}} d_{\mathrm{I}_{n,m},\mathrm{R}_l})^2}. \end{aligned} \tag{23}$$

The PL, assuming the conventional angle-based and the proposed angle-based trigonometric models with a single Tx/Rx, is demonstrated in Fig. 3 for different frequencies.

E. SINR *Formulation with Arbitrary Phase Shifts*

Next, we present the expression of T-I-R SINR for an IRS-aided network over the THz band. Assuming that $x_k(t)$ is the transmit signal of T_k at time slot t, the received signal $y_{\mathrm{T}_k,\mathrm{I}_n,\mathrm{R}_l}(t)$ at R_l is given in (24), at the top of next page, where the first part is the desired signal; interfering signals are represented in the second part; $w_l(t)$ denotes the additive white Gaussian noise (AWGN) at the user for the cascaded channel; $[\boldsymbol{\Theta}_n]_m = \kappa_{n,m} e^{j\theta_{n,m}}$ is the m^{th} element on the diagonal that

This work is licensed under a Creative Commons Attribution-NonCommercial-NoDerivatives 4.0 License. For more information, see https://creativecommons.org/licenses/by-nc-nd/4.0/

This article has been accepted for publication in IEEE Open Journal of the Communications Society. This is the author's version which has not been fully edited and content may change prior to final publication. Citation information: DOI 10.1109/OJCOMS.2024.3353173

$$
\begin{aligned}
y_{\mathrm{T}_k,\mathrm{I}_n,\mathrm{R}_l}(t) &= \sqrt{p_k}\widehat{h}_{\mathrm{T}_k,\mathrm{I}_n,\mathrm{R}_l}x_k(t) + \sum_{j=1,j\neq k}^{K}\sum_{i=1}^{N}\sqrt{p_j}\widehat{h}_{\mathrm{T}_j,\mathrm{I}_i,\mathrm{R}_l}x_j(t) + \sum_{j=1}^{K}\sum_{i=1}^{N}\sqrt{p_j}\widetilde{h}_{\mathrm{T}_j,\mathrm{I}_i,\mathrm{R}_l}x_j(t) + w_l(t) \\
&= \underbrace{\sqrt{p_k}(\widehat{\mathbf{h}}_{\mathrm{T}_k,\mathrm{I}_n})^T\boldsymbol{\Theta}_n\widehat{\mathbf{g}}_{\mathrm{I}_n,\mathrm{R}_l}x_k(t)}_{\text{desired signal}} + \underbrace{\sum_{j=1,j\neq k}^{K}\sum_{i=1}^{N}\sqrt{p_j}(\widehat{\mathbf{h}}_{\mathrm{T}_j,\mathrm{I}_i})^T\boldsymbol{\Theta}_i\widehat{\mathbf{g}}_{\mathrm{I}_i,\mathrm{R}_l}x_j(t)}_{\text{interference from another transmitters}} \\
&\quad + \underbrace{\sum_{j=1}^{K}\sum_{i=1}^{N}\sqrt{p_j}\big(\widetilde{\mathbf{h}}_{\mathrm{T}_j,\mathrm{I}_i}^T\boldsymbol{\Theta}_i\widehat{\mathbf{g}}_{\mathrm{I}_i,\mathrm{R}_l} + \widehat{\mathbf{h}}_{\mathrm{T}_j,\mathrm{I}_i}^T\boldsymbol{\Theta}_i\widetilde{\mathbf{g}}_{\mathrm{I}_i,\mathrm{R}_l} + \widetilde{\mathbf{h}}_{\mathrm{T}_j,\mathrm{I}_i}^T\boldsymbol{\Theta}_i\widetilde{\mathbf{g}}_{\mathrm{I}_i,\mathrm{R}_l}\big)x_j(t)}_{\text{interference due to imperfect CSI}} + \underbrace{w_l(t)}_{\text{noise}},
\end{aligned} \tag{24}
$$

$$
\begin{aligned}
\mathrm{SINR}_{\mathrm{T}_k,\mathrm{I}_n,\mathrm{R}_l} &= \frac{p_k\big|\widehat{h}_{\mathrm{T}_k,\mathrm{I}_n,\mathrm{R}_l}\big|^2}{\sum_{j=1,j\neq k}^{K}\sum_{i=1}^{N}p_j\big|\widehat{h}_{\mathrm{T}_j,\mathrm{I}_i,\mathrm{R}_l}\big|^2 + \sum_{j=1}^{K}\sum_{i=1}^{N}p_j\big|\widetilde{h}_{\mathrm{T}_j,\mathrm{I}_i,\mathrm{R}_l}\big|^2 + \sigma_l^2} \\
&= \frac{p_k\big|(\widehat{\mathbf{h}}_{\mathrm{T}_k,\mathrm{I}_n})^T\boldsymbol{\Theta}_n\widehat{\mathbf{g}}_{\mathrm{I}_n,\mathrm{R}_l}\big|^2}{\sum_{j=1,j\neq k}^{K}\sum_{i=1}^{N}p_j\big|(\widehat{\mathbf{h}}_{\mathrm{T}_j,\mathrm{I}_i})^T\boldsymbol{\Theta}_i\widehat{\mathbf{g}}_{\mathrm{I}_i,\mathrm{R}_l}\big|^2 + \sum_{j=1}^{K}\sum_{i=1}^{N}p_j\big(\sigma^2_{\widetilde{g}_{\mathrm{I}_i,\mathrm{R}_l}}\big|\widehat{\mathbf{h}}_{\mathrm{T}_j,\mathrm{I}_i}^T\widehat{\mathbf{h}}_{\mathrm{T}_j,\mathrm{I}_i}\big| + \sigma^2_{\widetilde{h}_{\mathrm{T}_j,\mathrm{I}_i}}\big|\widehat{\mathbf{g}}_{\mathrm{I}_i,\mathrm{R}_l}^T\widehat{\mathbf{g}}_{\mathrm{I}_i,\mathrm{R}_l}\big| + \sigma^2_{\widetilde{h}_{\mathrm{T}_j,\mathrm{I}_i}}\sigma^2_{\widetilde{g}_{\mathrm{I}_i,\mathrm{R}_l}}\big) + \sigma_l^2} \\
&= \frac{\frac{p_k\lambda^2}{16\pi^2}\Big|\sum_{m=1}^{M}\frac{\sqrt{\mathbb{G}_{\mathrm{T}_k}\mathbb{G}_{\mathrm{R}_l}\mathbb{G}_{\mathrm{I}_{n,m}}(-\mathbf{r}_{k,n,m})\mathbb{G}_{\mathrm{I}_{n,m}}(\mathbf{r}_{n,m,l})e^{-\kappa_{abs}(f)(d_{\mathrm{T}_k,\mathrm{I}_{n,m}}+d_{\mathrm{I}_{n,m},\mathrm{R}_l})}}}{d_{\mathrm{T}_k,\mathrm{I}_{n,m}}d_{\mathrm{I}_{n,m},\mathrm{R}_l}}\kappa_{n,m}e^{-j\frac{2\pi}{\lambda}(d_{\mathrm{T}_k,\mathrm{I}_{n,m}}+d_{\mathrm{I}_{n,m},\mathrm{R}_l})+j\theta_{n,m}}\Big|^2}{\sum_{j=1,j\neq k}^{K}\sum_{i=1}^{N}p_j\big|(\widehat{\mathbf{h}}_{\mathrm{T}_j,\mathrm{I}_i})^T\boldsymbol{\Theta}_i\widehat{\mathbf{g}}_{\mathrm{I}_i,\mathrm{R}_l}\big|^2 + \sum_{j=1}^{K}\sum_{i=1}^{N}p_j\big(\sigma^2_{\widetilde{g}_{\mathrm{I}_i,\mathrm{R}_l}}\big|\widehat{\mathbf{h}}_{\mathrm{T}_j,\mathrm{I}_i}^T\widehat{\mathbf{h}}_{\mathrm{T}_j,\mathrm{I}_i}\big| + \sigma^2_{\widetilde{h}_{\mathrm{T}_j,\mathrm{I}_i}}\big|\widehat{\mathbf{g}}_{\mathrm{I}_i,\mathrm{R}_l}^T\widehat{\mathbf{g}}_{\mathrm{I}_i,\mathrm{R}_l}\big| + \sigma^2_{\widetilde{h}_{\mathrm{T}_j,\mathrm{I}_i}}\sigma^2_{\widetilde{g}_{\mathrm{I}_i,\mathrm{R}_l}}\big) + \sigma_l^2},
\end{aligned} \tag{25}
$$

runs from the top left to the bottom right of matrix $\boldsymbol{\Theta}_n$. Thus, the SINR at R_l, $\mathrm{SINR}_{\mathrm{T}_k\mathrm{I}_n\mathrm{R}_l}$, of the desired signal from T_k-to-I_n-to-R_l link is given in (25), where σ_l^2 is the AWGN noise power at each receiver.

III. Problem Formulation

As stated earlier, our primary goal is T-I-R scheduling to maximize the sum rate. For our system model, the achievable rate can be written as

$$
R_{\mathrm{T}_k,\mathrm{I}_n,\mathrm{R}_l}([\boldsymbol{\Omega}]_{\mathrm{T}_k,\mathrm{I}_n,\mathrm{R}_l}) = \log_2(1+\mathrm{SINR}_{\mathrm{T}_k,\mathrm{I}_n,\mathrm{R}_l}([\boldsymbol{\Omega}]_{\mathrm{T}_k,\mathrm{I}_n,\mathrm{R}_l})). \tag{26}
$$

Considering the SINR as a function of $[\boldsymbol{\Omega}]_{\mathrm{T}_k,\mathrm{I}_n,\mathrm{R}_l}$, where $[\boldsymbol{\Omega}]_{\mathrm{T}_k,\mathrm{I}_n,\mathrm{R}_l}$ is the allocation matrix with each element of allocation matrix being a 3-dimension, i.e., $(\mathrm{T}_k,\mathrm{I}_n,\mathrm{R}_l)$. Therefore, the objective is to find the optimal allocation matrix $[\boldsymbol{\Omega}]_{\mathrm{T}_k,\mathrm{I}_n,\mathrm{R}_l}$ that maximizes the sum rate, expressed as

$$
\begin{aligned}
\underset{[\boldsymbol{\Omega}]_{\mathrm{T}_k,\mathrm{I}_n,\mathrm{R}_l},\boldsymbol{\Theta}_n}{\text{maximize}} \quad & \textstyle\sum_{l=1}^{L} R_{\mathrm{T}_k,\mathrm{I}_n,\mathrm{R}_l}([\boldsymbol{\Omega}]_{\mathrm{T}_k,\mathrm{I}_n,\mathrm{R}_l}), && \text{(27a)} \\
\text{subject to} \quad & \textstyle\sum_{k=1}^{K}[\boldsymbol{\Omega}]_{\mathrm{T}_k,\mathrm{I}_n,\mathrm{R}_l} = 1, \forall n,l, && \text{(27b)} \\
& \textstyle\sum_{n=1}^{N}[\boldsymbol{\Omega}]_{\mathrm{T}_k,\mathrm{I}_n,\mathrm{R}_l} = 1, \forall k,l, && \text{(27c)} \\
& \textstyle\sum_{l=1}^{L}[\boldsymbol{\Omega}]_{\mathrm{T}_k,\mathrm{I}_n,\mathrm{R}_l} = 1, \forall k,n, && \text{(27d)} \\
& [\boldsymbol{\Omega}]_{\mathrm{T}_k,\mathrm{I}_n,\mathrm{R}_l} \in \{0,1\}, \forall k,n,l, && \text{(27e)} \\
& \theta_{n,m} \in [0,2\pi), \kappa_{n,m} \leq 1, \forall n,m, && \text{(27f)}
\end{aligned}
$$

where the objective (27a) is the sum rate of the network given the pairing $[\boldsymbol{\Omega}]_{\mathrm{T}_k,\mathrm{I}_n,\mathrm{R}_l}$ with IRS reflection $\boldsymbol{\Theta}_n$; constraint (27b) ensures that each T will be paired to one I and R only; constraint (27c) guarantees that each I is allocated to one T and R; constraint (27d) make sure that each R is paired with one I and T. Thus, constraint (27b), (27c), and (27d) ensure a one-to-one T-I-R matching[5]. Additionally, constraint (27e) enforces that $[\boldsymbol{\Omega}]_{\mathrm{T}_k,\mathrm{I}_n,\mathrm{R}_l}$ is either 1 i.e., the IRS is allocated, or 0 i.e., the IRS is free and (27f) restricts the PS and amplitude of the reflection model. The formulated problem is a MINLP problem because it includes multiple integer variables, e.g., $[\boldsymbol{\Omega}]_{\mathrm{T}_k,\mathrm{I}_n,\mathrm{R}_l} \in \{0,1\}$, and continuous variables $\theta_{n,m} \in [0,2\pi]$, and the objective function is nonlinear [44–46]. Additionally, it can be observed that the optimization problem in (27) includes the optimization of the IRSs' reflection and a 3D matching problem involving three disjoint sets (i.e., Txs, IRSs, and Rxs). Thus, our MINLP problem in (27) is NP-hard since it combines optimizing over discrete variables with a challenge of dealing with nonlinear functions, and therefore its solution usually involves an enormous search space with exponential time complexity [47].

[5]We want to serve all T/R pairs, therefore, we allocate one IRS to assist the communication for one pair (T/R). Furthermore, multiple IRS allocations for one link cause a strong interference with the other links [24]. Thus, we allocate one IRS to serve one link in the network.

This work is licensed under a Creative Commons Attribution-NonCommercial-NoDerivatives 4.0 License. For more information, see https://creativecommons.org/licenses/by-nc-nd/4.0/

This article has been accepted for publication in IEEE Open Journal of the Communications Society. This is the author's version which has not been fully edited and content may change prior to final publication. Citation information: DOI 10.1109/OJCOMS.2024.3353173

IV. Optimal Solution and Problem Reformulation

With NP-hard problems, compute-intensive ES is conventionally used for finding the optimal solution [48]. As can be seen in (27), $\theta_{n,m}$ and $[\mathbf{\Omega}]_{\mathrm{T}_k,\mathrm{I}_n,\mathrm{R}_l}$ are functions of $(\mathrm{T}_k,\mathrm{I}_n,\mathrm{R}_l)$. Assuming that the imperfect CSI is available, we can obtain the optimal PS for any pairing, as explained next in (28). In this context, optimizing the PS and pairing are two independent problems. Thus, to address the optimization problem in (27), we search over all possible pairings, each pairing uses an optimal PS configuration to achieve the best potential performance of that pair. As a result, the obtained result is the optimal solution to problem (27). In what follows, we present the two steps of the optimal solution: (i) setting the optimal PS configuration for an arbitrary pair, i.e., a cascaded transmission from a T-to-I-to-R, and (ii) finding the optimal T-I-R parings for the entire network.

A. Phase Shift Optimization

Here, we optimize the reflection model to maximize the received signal strength by constructive addition of multiple reflected signals. In order to maximize the power gain, the PS induced by $\mathrm{I}_{n,m}$ is considered as an ideal PS configuration, and the amplitude of each IRS element is set to 1, as follows [36]

$$\theta^{\star}_{n,m} = \frac{2\pi}{\lambda}(d_{\mathrm{T}_k,\mathrm{I}_{n,m}} + d_{\mathrm{I}_{n,m},\mathrm{R}_l}), \tag{28}$$

$$\kappa^{\star}_{n,m} = 1, \forall n, m. \tag{29}$$

In the far-field $d_{\mathrm{T}_k,\mathrm{I}_{n,m}} > d_{ray}$, the distance $d_{\mathrm{T}_k,\mathrm{I}_{n,m}}$ using some basic algebra and first order Taylor expansion $(1+a)^x \approx 1+ax$, can be expressed as [36]

$$\begin{aligned} d_{\mathrm{T}_k,\mathrm{I}_{n,m}} \approx\ & d_{\mathrm{T}_k,\mathrm{I}_n} - m_x M_x \cos\phi^{\mathrm{inc}} \sin\psi^{\mathrm{rfl}} \\ & - m_y M_y \sin\phi^{\mathrm{inc}} \sin\psi^{\mathrm{rfl}}. \end{aligned} \tag{30}$$

For THz communications, the elements of the IRS are densely installed, and we ignore the distance between the IRS elements., which yields

$$d_{\mathrm{T}_k,\mathrm{I}_{n,m}} \approx d_{\mathrm{T}_k,\mathrm{I}_n}. \tag{31}$$

Similarly $d_{\mathrm{I}_{n,m},\mathrm{R}_l}$ can be written as

$$d_{\mathrm{I}_{n,m},\mathrm{I}_n} \approx d_{\mathrm{I}_n,\mathrm{R}_l}. \tag{32}$$

From (31) and (32), the PS in (28) is also valid for the far-field communication. Thus, the near-optimal PS configuration at I_n is determined as

$$\mathbf{\Theta}^{\star}_n = \mathrm{diag}[\kappa^{\star}_{n,1}e^{j\theta^{\star}_{n,1}}, .., \kappa^{\star}_{n,m}e^{j\theta^{\star}_{n,m}}, .., \kappa^{\star}_{n,M}e^{j\theta^{\star}_{n,M}}]. \tag{33}$$

As a result, the T-I-R SINR achieved by the near-optimal PS configuration can be expressed in (34), at the top of the next page.

Algorithm 1: Exhaustive Search Algorithm for Problem (27)

1 **Input:** N, K, $R_{\mathrm{T}_k,\mathrm{I}_n,\mathrm{R}_l}$, combination of set $C(N,K)$ as $\mathbf{C}_{temp}$, permutation of set K as $\mathbf{C}_{temp1}$, allocation matrix $[\mathbf{\Omega}]_{\mathrm{T}_k,\mathrm{I}_n,\mathrm{R}_l}$
2 **Initialize:** $[\mathbf{\Omega}]_{\mathrm{T}_k,\mathrm{I}_n,\mathrm{R}_l} = \emptyset$, $\sum R_{\mathrm{T}_k,\mathrm{I}_n,\mathrm{R}_l} = 0$
3 **for** $i \in \frac{N!}{(N-K)!}$ **do**
4 pairing T_k with k^{th} element of the i^{th} row in $\mathbf{C}_{temp}$ as $\mathrm{T}_k \leftarrow \mathbf{C}_{temp}(i,k)$
5 $\mathbf{C}_{temp}(i,k)$ gives the I_n
6 **for** $j \in L!$ **do**
7 pairing T_k with k^{th} element of the j^{th} row in $\mathbf{C}_{temp}$ as $\mathrm{T}_k \leftarrow \mathbf{C}_{temp}(j,k)$ $\mathbf{C}_{temp}(j,k)$ gives R_l
8 **for** $l \in K$ **do**
9 $\sum R_{\mathrm{T}_l,\mathrm{I}_n,\mathrm{R}_l}$ as in equation (26)
10 **if** $(\sum R_{\mathrm{T}_k,\mathrm{I}_n,\mathrm{R}_l} \geq \sum R^{\star}_{\mathrm{T}_k,\mathrm{I}_n,\mathrm{R}_l})$
11 $[\mathbf{\Omega}]^{\star}_{\mathrm{T}_k,\mathrm{I}_n,\mathrm{R}_l} \leftarrow [\mathbf{\Omega}]_{\mathrm{T}_k,\mathrm{I}_n,\mathrm{R}_l}$
12 **else**
13 $[\mathbf{\Omega}]^{\star}_{\mathrm{T}_k,\mathrm{I}_n,\mathrm{R}_l} \leftarrow [\mathbf{\Omega}]^{\star}_{\mathrm{T}_k,\mathrm{I}_n,\mathrm{R}_l}$
14 **Output:** optimal allocation matrix $[\mathbf{\Omega}]^{\star}_{\mathrm{T}_k,\mathrm{I}_n,\mathrm{R}_l}$

B. Optimal IRS Association using Exhaustive Search

In this subsection, we focus on the IRS pairing problem in (27) to find the optimal allocation matrix $[\mathbf{\Omega}]_{\mathrm{T}_k,\mathrm{I}_n,\mathrm{R}_l}$ with the sub-optimal reflection matrix $\mathbf{\Theta}^{\star}_n$ obtained from (33). In our ES method, the T-I-R sum rate with near-optimal PS is utilized to find the optimal pairing by checking all possible combinations and selecting the optimal one [49], [50]. Thus, in our model, we have $\frac{N!}{(N-K)!}$ combinations from T to I, and another $L!$ combinations from I to R, yielding $\frac{N!L!}{(N-K)!}$ combinations. The ES method for (27) is shown in Algorithm 1. The allocation matrix and the achievable rate are set to zero at the beginning of the algorithm. Then, we check all the $\frac{N!}{(N-K)!}$ combinations for the T to I links in the first for loop. In addition, for all combinations, we check the $L!$ combinations for the IRS to user links in the second for loop. Furthermore, if the sum rate of the current combination is greater than the existing combination, we select the current combination; otherwise, we keep the existing combination. This process is iterated until we check all combinations, thus reaching the optimal allocation matrix.

Remark 1. *The T-I-R allocation matrix obtained with the ES method as* $[\mathbf{\Omega}]^{\star}_{\mathrm{T}_k,\mathrm{I}_n,\mathrm{R}_l} = \underset{\mathrm{T}_k,\mathrm{I}_n,\mathrm{R}_l}{\arg\max}\{R_{\mathrm{T}_k,\mathrm{I}_n,\mathrm{R}_l}\}$ *converges to the global optimal solution of problem* (27).

Indeed, the optimality of the ES method can be proved by the following conditions. The ES method characteristics dictate that at every iteration, the sum rate for the current allocation matrix is calculated as in step 8 of Algorithm 1. In 9 to 12 of algorithm 1, we check if the sum rate of the current allocation matrix is greater than the previous one and select the one with a higher sum rate. In

This work is licensed under a Creative Commons Attribution-NonCommercial-NoDerivatives 4.0 License. For more information, see https://creativecommons.org/licenses/by-nc-nd/4.0/

This article has been accepted for publication in IEEE Open Journal of the Communications Society. This is the author's version which has not been fully edited and content may change prior to final publication. Citation information: DOI 10.1109/OJCOMS.2024.3353173

$$\mathrm{SINR}^{\mathrm{ideal}}_{\mathrm{T}_k,\mathrm{I}_n,\mathrm{R}_l}=\frac{\frac{p_k\lambda^2}{16\pi^2}\Big|\sum\limits_{m=1}^{M}\frac{\sqrt{\mathbb{G}_{\mathrm{T}_k}\mathbb{G}_{\mathrm{R}_l}\mathbb{G}_{\mathrm{I}_{n,m}}(-\mathbf{r}_{k,n,m})\mathbb{G}_{\mathrm{I}_{n,m}}(\mathbf{r}_{n,m,l})e^{-\kappa_{abs}(f)(d_{\mathrm{T}_k,\mathrm{I}_{n,m}}+d_{\mathrm{I}_{n,m},\mathrm{R}_l})}}}{d_{\mathrm{T}_k,\mathrm{I}_{n,m}}d_{\mathrm{I}_{n,m},\mathrm{R}_l}}\Big|^2}{\sum\limits_{\substack{j=1\\j\neq k}}^{K}\sum\limits_{i=1}^{N}p_j\big|(\widehat{\mathbf{h}}_{\mathrm{T}_j,\mathrm{I}_i})^T\boldsymbol{\Theta}_i\widehat{\mathbf{g}}_{\mathrm{I}_i,\mathrm{R}_l}\big|^2+\sum\limits_{j=1}^{K}\sum\limits_{i=1}^{N}p_j\big(\sigma^2_{\widetilde{g}_{\mathrm{I}_i,\mathrm{R}_l}}\big|\widehat{\mathbf{h}}^T_{\mathrm{T}_j,\mathrm{I}_i}\widehat{\mathbf{h}}_{\mathrm{T}_j,\mathrm{I}_i}\big|+\sigma^2_{\widetilde{h}_{\mathrm{T}_j,\mathrm{I}_i}}\big|\widehat{\mathbf{g}}^T_{\mathrm{I}_i,\mathrm{R}_l}\widehat{\mathbf{g}}_{\mathrm{I}_i,\mathrm{R}_l}\big|+\sigma^2_{\widetilde{h}_{\mathrm{T}_j,\mathrm{R}_i}}\sigma^2_{\widetilde{g}_{\mathrm{I}_i,\mathrm{R}_l}}\big)+\sigma^2_l}. \quad (34)$$

this way, we get the global optimal allocation matrix $[\boldsymbol{\Omega}]^{\star}_{\mathrm{T}_k,\mathrm{I}_n,\mathrm{R}_l}$, which gives the maximum sum rate.

Theorem 1. *Problem* (27) *is an NP-hard problem. Furthermore, problem* (27) *is NP-hard even if we only consider the T-I-R association with fixed PS at the IRSs.*

Proof: Based on the computational complexity theory, to show that problem (27) is NP-hard, we follow the following two steps: 1) select an appropriate known NP-hard problem, and 2) prove the optimization problem and the known NP-hard problem have the same objective values. First, 3D matching is known to be NP-hard. Then, considering an instant with fixed PS at the IRSs in (27) , which makes the optimization problem (27) a 3D matching problem. Therefore, the decision problem of the constructed instance is NP-complete, and the corresponding instance is NP-hard. Since a special case (i.e., with fixed PS) of problem (27) is NP-hard, the original problem in (27) is also NP-hard. ■

C. The Proposed Low-Complexity Solution

Every NP-complete problem can be solved by the ES method. However, when the size of the instances grows, the running time becomes forbiddingly large, even for instances of fairly small size. The complexity of the EC is exponential, and it is non-trivial to obtain an optimal matching in polynomial-time complexity. Therefore, we are motivated to design an efficient solution. Specifically, we first find the near-optimal IRS reflection coefficients and then decompose the 3D allocation problem into 2D sub-problems and reformulate the allocation optimization problem. The proposed solution is composed of two steps: (i) applying the near-optimal PS configuration in (33) for every possible pair and (ii) proposing a matching-theory-based low-complexity pairing algorithm. The roadmap for the proposed problem decomposition and the proposed algorithms to the corresponding sub-problems is shown in Fig. 4.

Since the IRS is neither a receiver nor a transmitter, $\Xi_{\mathrm{T}_k,\mathrm{I}_n,:}$ represents the pseudo SINRs from $\mathrm{T}_k\rightarrow\mathrm{I}_n$ estimated based on the imperfect CSI of the $\mathrm{T}_k\rightarrow\mathrm{I}_n$ link which can be expressed as

$$\Xi_{\mathrm{T}_k,\mathrm{I}_n,:}\triangleq\frac{p_k\big|(\widehat{\mathbf{h}}_{\mathrm{T}_k,\mathrm{I}_n})^T\widehat{\mathbf{h}}_{\mathrm{T}_k,\mathrm{I}_n}\big|}{\sum\limits_{\substack{j=1\\j\neq k}}^{K}p_j\big|(\widehat{\mathbf{h}}_{\mathrm{T}_j,\mathrm{I}_n})^T\widehat{\mathbf{h}}_{\mathrm{T}_j,\mathrm{I}_n}\big|+\sum\limits_{j=1}^{K}p_j\sigma^2_{\widetilde{h}_{\mathrm{T}_j,\mathrm{I}_n}}+\sigma^2}. \quad (35)$$

Here, the symbol ":" implies that the third dimension of $\boldsymbol{\Omega}$ is not taken into account. Furthermore, $\Xi_{\mathrm{T}_{k^\star},\mathrm{I}_{n^\star},\mathrm{R}_l}$ represents the pseudo SINR from $\mathrm{T}_{k^\star}\rightarrow\mathrm{I}_{n^\star}\rightarrow\mathrm{R}_l$ estimated based on the imperfect CSI of the network which can be expressed as

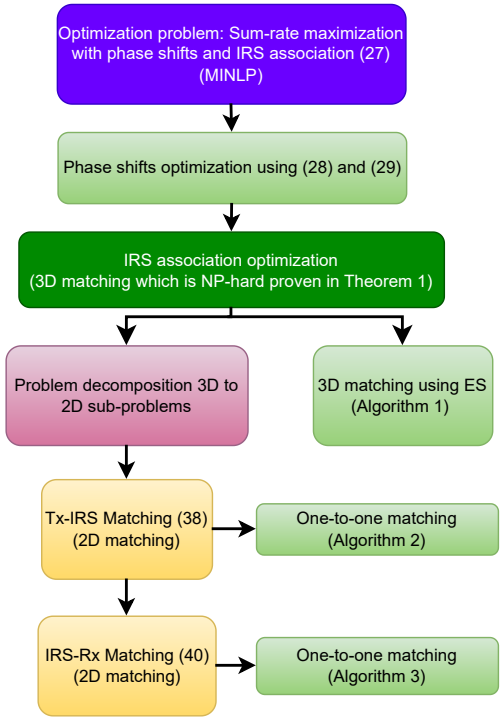


Fig. 4. A roadmap for the problem decomposition and the proposed algorithms.

$$\Xi_{\mathrm{T}_{k^\star},\mathrm{I}_{n^\star},\mathrm{R}_l}\triangleq\frac{p_{k^\star}\big|(\widehat{\mathbf{h}}_{\mathrm{T}_{k^\star},\mathrm{I}_{n^\star}})^T\boldsymbol{\Theta}_{n^\star}\widehat{\mathbf{g}}_{\mathrm{I}_{n^\star},\mathrm{R}_l}\big|^2}{\sum\limits_{\substack{j=1\\j\neq k}}^{K}\sum\limits_{i=1}^{N}p_j\big|(\widehat{\mathbf{h}}_{\mathrm{T}_j,\mathrm{I}_i})^T\boldsymbol{\Theta}_i\widehat{\mathbf{g}}_{\mathrm{I}_i,\mathrm{R}_l}\big|^2+\mathcal{X}+\sigma^2_l}, \quad (36)$$

where $\mathcal{X}=\sum\limits_{j=1}^{K}\sum\limits_{i=1}^{N}p_j\big(\sigma^2_{\widetilde{g}_{\mathrm{I}_i,\mathrm{R}_l}}\big|\widehat{\mathbf{h}}^T_{\mathrm{T}_j,\mathrm{I}_i}\widehat{\mathbf{h}}_{\mathrm{T}_j,\mathrm{I}_i}\big|+\sigma^2_{\widetilde{h}_{\mathrm{T}_j,\mathrm{I}_i}}\big|\widehat{\mathbf{g}}^T_{\mathrm{I}_i,\mathrm{R}_l}\widehat{\mathbf{g}}_{\mathrm{I}_i,\mathrm{R}_l}\big|+\sigma^2_{\widetilde{h}_{\mathrm{T}_j,\mathrm{I}_i}}\sigma^2_{\widetilde{g}_{\mathrm{I}_i,\mathrm{R}_l}}\big)$. We first introduce the following Lemma.

Lemma 2. *The pseudo sum rate achieved with allocation matrix obtained by the proposed algorithm for the decomposed sub-problems* $\sum\limits_{k^\star,n^\star,k}\Lambda_{\mathrm{T}_{k^\star},\mathrm{I}_{n^\star},\mathrm{R}_l}([\widehat{\boldsymbol{\Omega}}]^{\star}_{\mathrm{T}_k,\mathrm{I}_n,\mathrm{R}_l})$ *is a sub-optimal solution to problem* (27)*, upper bounded by the sum rate achieved with allocation matrix obtained by the ES method* $\sum\limits_{\mathrm{T}_k,\mathrm{I}_n,\mathrm{R}_l}R_{\mathrm{T}_k,\mathrm{I}_n,\mathrm{R}_l}([\boldsymbol{\Omega}]^{\star}_{\mathrm{T}_k,\mathrm{I}_n,\mathrm{R}_l})$.

Proof: The proof is given in Appendix B ■

This work is licensed under a Creative Commons Attribution-NonCommercial-NoDerivatives 4.0 License. For more information, see https://creativecommons.org/licenses/by-nc-nd/4.0/

This article has been accepted for publication in IEEE Open Journal of the Communications Society. This is the author's version which has not been fully edited and content may change prior to final publication. Citation information: DOI 10.1109/OJCOMS.2024.3353173

Invoking Lemma 2, the original problem can be decomposed into two sub-problems, where the obtained solutions are sub-optimal solution to problem (27).

1) Tx-IRS Matching Problem: Considering the T-I matching as a bipartite graph matching problem, we take into account the first and second dimensions of $\mathbf{\Omega}$. From the relationship in (55), we define the following pseudo quantity to represent the potential sum rate of the incident channels

$$\Lambda_{\mathrm{T}_k,\mathrm{I}_n,:}([\mathbf{\Omega}]_{\mathrm{T}_k,\mathrm{I}_n,:}) \triangleq \log_2(1+\Xi_{\mathrm{T}_k,\mathrm{I}_n,:}([\mathbf{\Omega}]_{\mathrm{T}_k,\mathrm{I}_n,:})). \tag{37}$$

Using (37), the first sub-problem of the decomposed problem can be expressed as

$$\begin{aligned}
\underset{[\mathbf{\Omega}]_{\mathrm{T}_k,\mathrm{I}_n,:}}{\text{maximize}} \quad & \textstyle\sum_{k=1}^{K} \Lambda_{\mathrm{T}_k,\mathrm{I}_n,:}([\mathbf{\Omega}]_{\mathrm{T}_k,\mathrm{I}_n,:}), && \text{(38a)}\\
\text{subject to} \quad & \textstyle\sum_{k=1}^{K}[\mathbf{\Omega}]_{\mathrm{T}_k,\mathrm{I}_n,:}=1,\forall n, && \text{(38b)}\\
& \textstyle\sum_{n=1}^{N}[\mathbf{\Omega}]_{\mathrm{T}_k,\mathrm{I}_n,:}=1,\forall k, && \text{(38c)}\\
& [\mathbf{\Omega}]_{\mathrm{T}_k,\mathrm{I}_n,:}=\{0,1\},\forall k,n, && \text{(38d)}
\end{aligned}$$

where $[\mathbf{\Omega}]_{\mathrm{T}_k,\mathrm{I}_n,:}$ is the allocation matrix where each element is a 2-dimension, i.e., in this phase, the transmitter to IRS allocation is perform. The constraint (38b) ensures that each T_k is paired to one I_n only. Constraint (38c) guarantees that each IRS is allocated to one transmitter. Thus, constraint (38b) and (38c) ensure a one-to-one T-I matching. In this phase we achieve the matching between $\mathrm{T}_{k^\star}$ and $\mathrm{I}_{n^\star}$, and the achieved allocation matrix can be denoted as $[\mathbf{\Omega}]_{\mathrm{T}_{k^\star},\mathrm{I}_{n^\star},:}$.

2) IRS-Rx Matching Problem: After pairing T-I, the allocation matrix $[\mathbf{\Omega}]_{\mathrm{T}_{k^\star},\mathrm{I}_{n^\star},:}$ is utilize and consider as $\mathrm{T}_{k^\star}$ is paired with $\mathrm{I}_{n^\star}$. Consequently, we formulate the I-R pairing problem to maximize the pseudo sum rate in this phase as follows

$$\begin{aligned}
&\Lambda_{\mathrm{T}_{k^\star},\mathrm{I}_{n^\star},\mathrm{R}_l}([\mathbf{\Omega}]_{\mathrm{T}_{k^\star},\mathrm{I}_{n^\star},\mathrm{R}_l})\\
&\qquad \triangleq \log_2(1+\Xi_{\mathrm{T}_{k^\star},\mathrm{R}_n^\star,\mathrm{R}_l}([\mathbf{\Omega}]_{\mathrm{T}_{k^\star},\mathrm{I}_{n^\star},\mathrm{R}_l})).
\end{aligned} \tag{39}$$

Using (39), the second sub-problem can be formulated as

$$\begin{aligned}
\underset{[\mathbf{\Omega}]_{\mathrm{T}_{k^\star},\mathrm{I}_{n^\star},\mathrm{R}_l}}{\text{maximize}} \quad & \textstyle\sum_{l=1}^{L} \Lambda_{\mathrm{T}_{k^\star},\mathrm{I}_{n^\star},\mathrm{R}_l}([\mathbf{\Omega}]_{\mathrm{T}_{k^\star},\mathrm{I}_{n^\star},\mathrm{R}_l}), && \text{(40a)}\\
\text{subject to} \quad & \textstyle\sum_{n^\star=1}^{N}[\mathbf{\Omega}]_{\mathrm{T}_{k^\star},\mathrm{I}_{n^\star},\mathrm{R}_l}=1,\forall k, && \text{(40b)}\\
& \textstyle\sum_{l=1}^{L}[\mathbf{\Omega}]_{\mathrm{T}_{k^\star},\mathrm{I}_{n^\star},\mathrm{R}_l}=1,\forall n^\star, && \text{(40c)}\\
& [\mathbf{\Omega}]_{\mathrm{T}_{k^\star},\mathrm{I}_{n^\star},\mathrm{R}_l}=\{0,1\},\forall n^\star,k, && \text{(40d)}
\end{aligned}$$

where $[\mathbf{\Omega}]_{\mathrm{T}_{k^\star},\mathrm{I}_{n^\star},\mathrm{R}_l}$ is the allocation matrix from I-R link with obtained T-I allocation matrix from first sub-problem. Constraint (40b) ensures that each IRS $\mathrm{I}_{n^\star}$ is paired to only one Rx R_l and (40c) guarantees that each IRS is allocated to one Rx. Thus, (40b) and (40c) ensure a one-to-one matching. The implementation of the proposed algorithm is presented in what follows.

V. Proposed Gale-Shapley Algorithm-based Solution

IRS-aided networks require a massive number of reflecting elements M, especially at higher frequencies, when the number of elements can reach 100×100. In this context, our model contains multiple distributed IRSs with a large number of reflecting elements. Thus, the ES method is not an efficient scheme, even for 2D allocation problems. Therefore, to optimize the 2D allocation problems in (38) and (40), we propose a Gale-Shapley algorithm based [51] solution, presented in the following sections.

Definition 1. *A one-to-one matching between two disjoint sets K and N can be represented by a one-to-one correspondence $\mu(.)$, where $k\in K$ is mapped to $n\in N$ if and only if n is also mapped to k, i.e., $m=\mu(n)$ and $n=\mu(m)$.*

A. Phase I: Tx-IRS Matching Problem

The proposed scheme for (38) is elaborated in two stages: configuration of a priority matrix at Tx and IRS for each T-I link, and T-I allocation as a matching problem.

1) Tx and IRS Priority Matrix Configuration: The first sub-problem, i.e., (38), seeks to maximize a pseudo quantity between T-I link through T-I pairing. The pseudo quantity between T_k and I_n is denoted as $\Lambda_{\mathrm{T}_k,\mathrm{I}_n,:}$, and given as

$$\Lambda_{\mathrm{T}_k,\mathrm{I}_n,:} \triangleq \log_2(1+\Xi_{\mathrm{T}_k,\mathrm{I}_n,:}). \tag{41}$$

The transmitter priorities are obtained based on the pseudo quantity $\Lambda_{\mathrm{T}_k,\mathrm{I}_n,:}$ between each IRS and the transmitter. After calculating the pseudo quantity between each transmitter and all the IRSs, and storing them in a matrix $[\mathbf{\Lambda}]^{\mathrm{T}}_{\mathrm{T}_k,\mathrm{I}_n,:}$, the transmitter priority matrix is constructed. Furthermore, the channel reciprocity holds for the T-I channel [33], thus the pseudo quantity between each IRS and all the transmitters is the transpose of the matrix $[\mathbf{\Lambda}]^{\mathrm{T}}_{\mathrm{T}_k,\mathrm{I}_n,:}$, which we denote as $[\mathbf{\Lambda}]^{\mathrm{I}}_{\mathrm{I}_n,\mathrm{T}_k,:}$. The priority matrix at transmitters/IRSs is constructed with the highest pseudo quantity offered by the IRSs/transmitters at the top and the lowest pseudo quantity offered by the one at the bottom, as shown in Algorithm 2 steps 2 to 6. Additionally, the dimension of the transmitter priority matrix $[\mathbf{\Upsilon}]^{\mathrm{T}}_{\mathrm{T}_k,\mathrm{I}_n,:}$ is $K\times N$ and the IRS priority matrix $[\mathbf{\Upsilon}]^{\mathrm{I}}_{\mathrm{I}_n,\mathrm{T}_k,:}$ is $N\times K$. The priority relations for the ***proposer*** to the ***responders*** are defined in Definition 2.

Definition 2. *The **proposer** P prefers the **responder** R to the **responder** $R^\star$ is denoted as $R\succ^P R^\star$, where $R\neq R^\star$, if $\Lambda_{R,P}>\Lambda_{R^\star,P}$.*

2) Proposed Tx-IRS Allocation Algorithm: We deploy a large number of IRSs in the network to assist the communication and assume that the number of IRSs is greater than the number of Txs (i.e., $N>K$). We explore T-I allocation algorithms as one-to-one matching in the first phase of our proposal. Each transmitter can be allocated to at most one IRS in one-to-one matching. The remaining IRSs, which are not allocated to any transmitter, are considered inactive for this round. The algorithm, shown in Algorithm 2, is illustrated as a series of attempts from transmitters to IRSs. The IRS can either be associated with the transmitter or remain vacant during this process. Each transmitter node proposes pairing with the highest priority IRS in their priority list until the transmitter has either been paired or rejected by all IRS. Transmitters rejected by the IRS are not allowed to try again for the same IRS. The IRS is immediately engaged if the transmitter

This work is licensed under a Creative Commons Attribution-NonCommercial-NoDerivatives 4.0 License. For more information, see https://creativecommons.org/licenses/by-nc-nd/4.0/

This article has been accepted for publication in IEEE Open Journal of the Communications Society. This is the author's version which has not been fully edited and content may change prior to final publication. Citation information: DOI 10.1109/OJCOMS.2024.3353173

Algorithm 2: Proposed Tx-IRS Allocation Algorithm for Problem (38)

Input: K, N, $\Lambda^{\mathrm{T}}_{\mathrm{T}_k,\mathrm{I}_n,:}$, $\Lambda^{\mathrm{I}}_{\mathrm{I}_n,\mathrm{T}_k,:}$, $[\boldsymbol{\Upsilon}]^{\mathrm{T}}_{\mathrm{T}_k,\mathrm{I}_n,:}$, $[\boldsymbol{\Upsilon}]^{\mathrm{I}}_{\mathrm{I}_n,\mathrm{T}_k,:}$, set of unmatched transmitters Π_{T}, $[\boldsymbol{\Omega}]_{\mathrm{T}_k,\mathrm{I}_n,:}$

Initialize $[\boldsymbol{\Upsilon}]^{\mathrm{T}}_{\mathrm{T}_k,\mathrm{I}_n,:} = \emptyset$, $[\boldsymbol{\Upsilon}]^{\mathrm{I}}_{\mathrm{I}_n,\mathrm{T}_k,:} = \emptyset$, $[\boldsymbol{\Omega}]_{\mathrm{T}_k,\mathrm{I}_n,:} = \emptyset$;

Priority Matrix Configuration:

for $k \in K$ **do**

  $\Lambda_{\mathrm{T}_k,\mathrm{I}_n,:}, \quad \forall\ n \in N$ and store in $[\boldsymbol{\Lambda}]^{\mathrm{T}}_{\mathrm{T}_k,\mathrm{I}_n,:}$

$[\boldsymbol{\Lambda}]^{\mathrm{I}}_{\mathrm{I}_n,\mathrm{T}_k,:} = [[\boldsymbol{\Lambda}]^{\mathrm{T}}_{\mathrm{T}_k,\mathrm{I}_n,:}]^T$

$[[\boldsymbol{\Lambda}]^{\mathrm{T}}_{\mathrm{T}_k,\mathrm{I}_n,:},[\boldsymbol{\Upsilon}]^{\mathrm{T}}_{\mathrm{T}_k,\mathrm{I}_n,:}]$ = sort $([\boldsymbol{\Lambda}]^{\mathrm{T}}_{\mathrm{T}_k,\mathrm{I}_n,:}$,2,descend)

$[[\boldsymbol{\Lambda}]^{\mathrm{I}}_{\mathrm{I}_n,\mathrm{T}_k,:},[\boldsymbol{\Upsilon}]^{\mathrm{I}}_{\mathrm{I}_n,\mathrm{T}_k,:}]$ = sort $([\boldsymbol{\Lambda}]^{\mathrm{I}}_{\mathrm{I}_n,\mathrm{T}_k,:}$,2,descend)

Tx-IRS Allocation:

while *(either* $\Pi_{\mathrm{T}} \neq \emptyset$ *or transmitters not rejected by all IRSs)* **do**

  for $\mathrm{T}_{k'} \in \Pi_{\mathrm{T}}$ **do**

    propose to the highest priority IRS in $[\boldsymbol{\Upsilon}]^{\mathrm{T}}_{\mathrm{T}_k,\mathrm{I}_n,:}$

    element of $[\boldsymbol{\Omega}]_{\mathrm{T}_k,\mathrm{I}_n,:} = 1$

  for $\mathrm{I}_n \in N$ **do**

    if $(\mathrm{I}_n \notin [\boldsymbol{\Omega}]_{\mathrm{T}_k,\mathrm{I}_n,:}$)

    $[\boldsymbol{\Omega}]_{\mathrm{T}_k,\mathrm{I}_n,:} \leftarrow [\boldsymbol{\Omega}]_{\mathrm{T}_k,\mathrm{I}_n,:} \cup (\mathrm{T}_{k'}, \mathrm{I}_n)$

    else if $(\Lambda^{\mathrm{I}}_{\mathrm{I}_n,\mathrm{T}_{k'},:} > \Lambda^{\mathrm{I}}_{\mathrm{I}_n,\mathrm{T}_k,:})$

    $[\boldsymbol{\Omega}]_{\mathrm{T}_k,\mathrm{I}_n,:} \leftarrow [\boldsymbol{\Omega}]_{\mathrm{T}_k,\mathrm{I}_n,:} \cup (\mathrm{T}_{k'}, \mathrm{I}_n)$

    else

    $[\boldsymbol{\Omega}]_{\mathrm{T}_k,\mathrm{I}_n,:} \leftarrow [\boldsymbol{\Omega}]_{\mathrm{T}_k,\mathrm{I}_n,:} \cup (\mathrm{T}_k, \mathrm{I}_n)$

Output: T-I allocation matrix $[\overline{\boldsymbol{\Omega}}]_{\mathrm{T}_{k^\star},\mathrm{I}_{n^\star},:}$

proposes a free IRS; however, if the transmitter proposes an IRS that is already engaged, the IRS compares the new and current transmitter and gets engaged with the best one, i.e., the one with higher pseudo quantity link. Thus, if the IRS favors the current transmitter, the new proposal will be rejected. Alternatively, if the IRS prefers the new proposal, then the IRS will break the engagement with the current transmitter and accept the new one. The process is repeated until all transmitter are engaged or all options are considered.

Lemma 3. *The proposed **proposer-responder** allocation algorithm terminates in polynomial time, i.e., if there are K **proposers** and N **responders** then the algorithm is terminated after at most $K \times N$ iterations.*

Proof: In each iteration, each unmatched ***proposer*** proposes to a ***responder*** that it has never explored before. Moreover, the ***responder*** accepts or rejects the new proposal according to the status and preference of the ***responder***. As a result, for N ***responders*** and K ***proposers***, we have $K \times N$ possible proposals occuring in the proposed algorithm. This completes the proof of Lemma 3. ∎

Lemma 4. *If **proposer** P pairs with **responder** R in the i^{th} iteration, then in every subsequent iteration, **responder** R pairs with a proposer which is at least as good as P.*

Proof: The proof is given in Appendix C. ∎

Theorem 2. *The **proposer-responder** matching achieved for each phase of the proposed algorithm returns a stable matching. Furthermore, the stability is not affected by inverting the proposing order.*

Proof: The proof is given in Appendix D. ∎

B. Phase II: (Tx, IRS)-Rx Matching Problem

The allocation matrix obtained in subsection V-A can be used to achieve the I-R allocation matrix. In this way, we achieve the T-I-R allocation matrix as a sub-optimal solution.

1) IRS and Rx Priority Matrix Configuration: Considering that $(\mathrm{T}_{k^\star}, \mathrm{I}_{n^\star})$ is the pair obtained in the T-I allocation, the data rate offered by R_k to the $(\mathrm{T}_{k^\star}, \mathrm{I}_{n^\star})$ channel is given as

$$\Lambda_{\mathrm{T}_{k^\star},\mathrm{I}_{n^\star},\mathrm{R}_k} \triangleq \log_2(1 + \Xi_{\mathrm{T}_{k^\star},\mathrm{I}_{n^\star},\mathrm{R}_l}). \tag{42}$$

Combining all the data rates between IRSs and receivers yields a data rate matrix, $[\boldsymbol{\Lambda}]^{\mathrm{I}}_{\mathrm{T}_{k^\star},\mathrm{I}+n^\star,\mathrm{R}_l}$, and the date rate matrix between each receiver to all the IRSs, $[\boldsymbol{\Lambda}]^{\mathrm{R}}_{\mathrm{T}_{k^\star},\mathrm{R}_l,\mathrm{I}_{n^\star}}$, is the transpose of $[\boldsymbol{\Lambda}]^{\mathrm{I}}_{\mathrm{T}_{k^\star},\mathrm{I}_{n^\star},\mathrm{R}_l}$. In this context, the priority matrix is created in descending order of priorities. Accordingly, the Rx/IRS with the highest priority comes first for each IRS/Rx in the priority matrix. The priority matrix for IRSs and receivers, which we represent as $[\boldsymbol{\Upsilon}]^{\mathrm{I}}_{\mathrm{T}_{k^\star},\mathrm{I}_{n^\star},\mathrm{R}_l}$ and $[\boldsymbol{\Upsilon}]^{\mathrm{R}}_{\mathrm{T}_{k^\star},\mathrm{R}_l,\mathrm{I}_{n^\star}}$, can be calculated as shown in Algorithm 3 steps 2 to 6, respectively.

2) Proposed Rx-IRS Allocation Algorithm: After getting the T-I allocation matrix $[\overline{\boldsymbol{\Omega}}]_{\mathrm{T}_{k^\star},\mathrm{I}_{n^\star}}$ in the first phase, we propose a matching algorithm, for R-I allocation. We assume that the number of active IRSs and receivers are similar in this phase, and therefore we investigate R-I allocation algorithms as one-to-one matching. The algorithm is illustrated as a series of attempts from receivers to IRSs. The IRS can either be paired with the Rx or remain vacant during this process. A Rx proposes for matching with the highest priority IRS in their priority list until the Rx has been allocated or rejected by each IRS. Receivers rejected by the IRS are not allowed to try again for the same IRS. The IRS is immediately engaged if the Rx proposes a free IRS. However, if the Rx proposes to the already engaged IRS, then the IRS compares the new and current receivers and gets engaged with the one with highest data rate link. This process continues until all receivers are engaged, or all options have been explored.

C. Case Study of The Proposed Solution

In the first phase, T-I allocation is considered for $K = 3$ and $N = 4$. The priority matrices between the Tx and the IRS and IRS and Tx are tabulated in Tables IV(a) and Table IV(b), respectively. The transmitters attempt the IRS based on their priorities. In the first round, transmitters target the 1^{st} choice IRS as, T_1, T_2, and T_3 try for I_1, I_1, and I_2, respectively. At this stage, all the IRSs are free, so if an IRS gets one proposal, it accept it and if it gets more than one proposal, it checks the priority of the proposing transmitters and accepts the one with the highest priority. Here, I_2 receive one proposal, thus I_2 accept the proposal i.e., T_3. However, T_1 and T_2 both want to pair with I_1, which checks

This work is licensed under a Creative Commons Attribution-NonCommercial-NoDerivatives 4.0 License. For more information, see https://creativecommons.org/licenses/by-nc-nd/4.0/

This article has been accepted for publication in IEEE Open Journal of the Communications Society. This is the author's version which has not been fully edited and content may change prior to final publication. Citation information: DOI 10.1109/OJCOMS.2024.3353173

Algorithm 3: Proposed Rx-IRS Allocation Algorithm for Problem (40)

Input: L, $\Lambda^{\mathrm{I}}_{\mathrm{T}_{k^\star},\mathrm{I}_{n^\star},\mathrm{R}_l}$,$\Lambda^{\mathrm{R}}_{\mathrm{T}_{k^\star},\mathrm{R}_k,\mathrm{I}_{n^\star}}$, $[\boldsymbol{\Upsilon}]^{\mathrm{R}}_{\mathrm{T}_{k^\star},\mathrm{R}_l,\mathrm{I}_{n^\star}}$, $[\boldsymbol{\Upsilon}]^{\mathrm{I}}_{\mathrm{T}_{k^\star},\mathrm{I}_{n^\star},\mathrm{R}_l}$, set of unmatched receivers Π_{R}, $[\boldsymbol{\Omega}]_{\mathrm{T}_{k^\star},\mathrm{I}_{n^\star},\mathrm{R}_l}$

Initialize $[\boldsymbol{\Upsilon}]^{\mathrm{I}}_{\mathrm{T}_{k^\star},\mathrm{I}_{n^\star},\mathrm{R}_l} = \emptyset$, $[\boldsymbol{\Upsilon}]^{\mathrm{R}}_{\mathrm{T}_{k^\star},\mathrm{R}_l,\mathrm{I}_{n^\star}} = \emptyset$, $[\boldsymbol{\Omega}]_{\mathrm{T}_{k^\star},\mathrm{I}_{n^\star},\mathrm{R}_l} = \emptyset$;

Priority Matrix Configuration:

for $l \in L$ **do**

  $\Lambda_{\mathrm{T}_{k^\star},\mathrm{I}_{n^\star},\mathrm{R}_l}, \quad \forall\ k \in K$ and store in $[\boldsymbol{\Lambda}]^{\mathrm{I}}_{\mathrm{T}_{k^\star},\mathrm{I}_{n^\star},\mathrm{R}_k}$

$[\boldsymbol{\Lambda}]^{\mathrm{R}}_{\mathrm{T}_{k^\star},\mathrm{R}_l,\mathrm{I}_{n^\star}} = [[\boldsymbol{\Lambda}]^{\mathrm{I}}_{\mathrm{T}_{k^\star},\mathrm{I}_{n^\star},\mathrm{R}_l}]^T$

$[[\boldsymbol{\Lambda}]^{\mathrm{I}}_{\mathrm{T}_{k^\star},\mathrm{I}_{n^\star},\mathrm{R}_l},[\boldsymbol{\Upsilon}]^{\mathrm{I}}_{\mathrm{T}_{k^\star},\mathrm{I}_{n^\star},\mathrm{R}_l}]$ = sort $([\boldsymbol{\Lambda}]^{\mathrm{I}}_{\mathrm{T}_{k^\star},\mathrm{I}_{n^\star},\mathrm{R}_l}$,2,descend)

$[[\boldsymbol{\Lambda}]^{\mathrm{R}}_{\mathrm{T}_{k^\star},\mathrm{R}_l,\mathrm{I}_{n^\star}},[\boldsymbol{\Upsilon}]^{\mathrm{R}}_{\mathrm{T}_{k^\star},\mathrm{R}_l,\mathrm{I}_{n^\star}}]$ = sort $([\boldsymbol{\Lambda}]^{\mathrm{R}}_{\mathrm{T}_{k^\star},\mathrm{R}_l,\mathrm{I}_{n^\star}}$,2,descend)

Rx-IRS Allocation:

while *(either* $\Pi_{\mathrm{R}} \neq \emptyset$ *or receivers not rejected by all IRSs)* **do**

  for $\mathrm{R}_{k'} \in \Pi_{\mathrm{R}}$ **do**

    propose to the highest priority IRS in $[\boldsymbol{\Upsilon}]^{\mathrm{R}}_{\mathrm{T}_{k^\star},\mathrm{R}_l,\mathrm{I}_{n^\star}}$

    element of $[\boldsymbol{\Omega}]_{\mathrm{T}_{k^\star},\mathrm{I}_{n^\star},\mathrm{R}_l} = 1$, Remove $\mathrm{I}_{n^\star}$ from $[\boldsymbol{\Upsilon}]^{\mathrm{I}}_{\mathrm{T}_{k^\star},\mathrm{I}_{n^\star},\mathrm{R}_l}$

  for $\mathrm{I}_{n^\star} \in L$ **do**

    if $(\mathrm{I}_{n^\star} \notin [\boldsymbol{\Omega}]_{\mathrm{R}_{k^\star},\mathrm{I}_{n^\star},\mathrm{R}_l}$)

    $[\boldsymbol{\Omega}]_{\mathrm{T}_{k^\star},\mathrm{I}_{n^\star},\mathrm{R}_l} \leftarrow [\boldsymbol{\Omega}]_{\mathrm{T}_{k^\star},\mathrm{I}_{n^\star},\mathrm{R}_l} \cup (\mathrm{I}_{n^\star},\mathrm{R}_{k'})$

    else if $(\Lambda^{\mathrm{I}}_{\mathrm{T}_{k^\star},\mathrm{I}_{n^\star},\mathrm{R}_{k'}} > \Lambda^{\mathrm{I}}_{\mathrm{T}_{k^\star},\mathrm{I}_{n^\star},\mathrm{R}_k})$

    $[\boldsymbol{\Omega}]_{\mathrm{T}_{k^\star},\mathrm{I}_{n^\star},\mathrm{R}_l} \leftarrow [\boldsymbol{\Omega}]_{\mathrm{T}_{k^\star},\mathrm{I}_{n^\star},\mathrm{R}_l} \cup (\mathrm{I}_{n^\star},\mathrm{R}_{k'})$

    else

    $[\boldsymbol{\Omega}]_{\mathrm{T}_{k^\star},\mathrm{I}_{n^\star},\mathrm{R}_l} \leftarrow [\boldsymbol{\Omega}]_{\mathrm{T}_{k^\star},\mathrm{I}_{n^\star},\mathrm{R}_l} \cup (\mathrm{I}_{n^\star},\mathrm{R}_k)$

Output: T-I-R allocation matrix $[\overline{\boldsymbol{\Omega}}]^{\star}_{\mathrm{T}_k,\mathrm{I}_n,\mathrm{R}_l}$

its priority list before accepting the proposals. In this context, since the priority of T_1 is higher than that of T_2, I_1 accept T_1 and reject T_2. Therefore, in the second round, T_2 proposes to the next IRS on its priority list, which is I_2. Since I_2 is already paired, I_2 checks its preference between existing and new proposal. Here, the priority of T_2 is high, and so I_2 break the existing pair and accept with T_2. In the third round, T_3 proposes the next IRS available for pairing in its priority list, thus I_3 is allocate to T_3. This process is shown in Table IV(c), where $\mathtt{CUR}(\mathrm{T})$ is the highest-ranked IRS in the transmitter list that has not been rejected yet and the list of unmatched transmitters are placed in $\mathtt{LIST}$. After allocating all transmitters, we consider the remaining IRSs in the $\mathtt{LIST}$, which are not allocated as inactive IRSs for the second sub-problem. The graphic view of the T-I matched is shown in Fig. 5.

To demonstrate the second sub-problem after getting the first phase results, we consider an imaginary set of priorities for receivers and IRSs. The priorities of receivers and IRSs' are tabulated in Tables V(a) and V(b), respectively. In the first round, receivers target the 1^{st} choice IRS, where R_1 try for I_2, while R_2, and R_3 explore I_1. Here, I_2 being free and targeted by one R so it accept the proposal, while I_1 checks its priority list before accepting the proposals. Thus, for I_1, R_3's proposal is accepted since its priority is higher than that of R_2. In the second round, R_2 chooses the next IRS in their priority list, i.e., I_2. Since the targeted IRS is allocated to R_1, I_2 checks its priority and accept the new proposal and break the existing allocation since its priority is higher than the existing one. In the third round, R_1 target I_1, which is engaged with R_3. Thus, I_1 checks its priority and reject the new proposal since its existing allocated partner priority is higher than the new proposal. Furthermore, in the fourth round, R_1 chooses I_3, and the proposal is accepted since I_3 is vacant. This process is shown in Table V(c). After solving both sub-problems the result to the T-I-R allocation is mapped as $(\mathrm{T}_1 \rightarrow \mathrm{I}_1 \rightarrow \mathrm{R}_3)$, $(\mathrm{T}_2 \rightarrow \mathrm{I}_2 \rightarrow \mathrm{R}_2)$, and $(\mathrm{T}_3 \rightarrow \mathrm{I}_3 \rightarrow \mathrm{R}_1)$. The graphic view of the T-I-R matched is shown in Fig. 6.

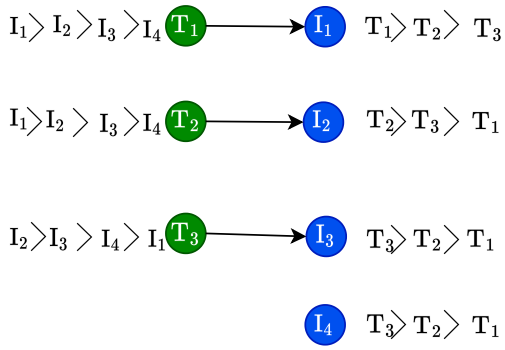


Fig. 5. The graph of the Tx - IRS matching problem.

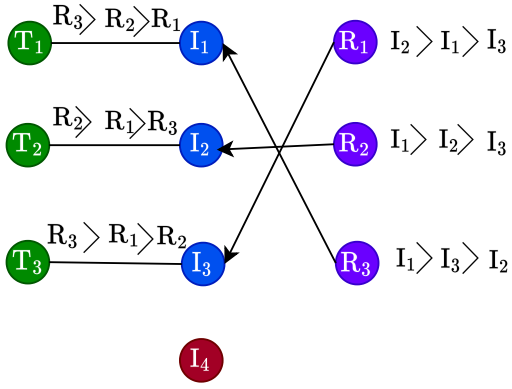


Fig. 6. The graph of the (Tx, IRS) - Rx matching problem.

This work is licensed under a Creative Commons Attribution-NonCommercial-NoDerivatives 4.0 License. For more information, see https://creativecommons.org/licenses/by-nc-nd/4.0/

This article has been accepted for publication in IEEE Open Journal of the Communications Society. This is the author's version which has not been fully edited and content may change prior to final publication. Citation information: DOI 10.1109/OJCOMS.2024.3353173

TABLE IV
PRIORITY MATRIX OF TRANSMITTERS, IRSS, AND ALLOCATION ROUNDS OF 1^{st} PHASE FROM TX TO IRS

	1^{st} Choice		2^{nd} Choice		3^{rd} Choice		4^{th} Choice	
	I	Eq.(41)	I	Eq.(41)	I	Eq.(41)	I	Eq.(41)
T_1	I_1	0.623	I_2	0.134	I_3	0.026	I_4	0.012
T_2	I_1	0.505	I_2	0.448	I_3	0.044	I_4	0.022
T_3	I_2	0.203	I_3	0.160	I_4	0.157	I_1	0.025

(a)

	1^{st} Choice		2^{nd} Choice		3^{rd} Choice	
	T_k	Eq.(41)	T_k	Eq.(41)	T_k	Eq.(41)
I_1	T_1	0.623	T_2	0.504	T_3	0.025
I_2	T_2	0.448	T_3	0.203	T_1	0.134
I_3	T_3	0.160	T_2	0.044	T_1	0.026
I_4	T_3	0.157	T_2	0.022	T_1	0.012

(b)

	I_1	I_2	I_3	I_4	$\sum \Lambda_{T_k,I_n,:}$	LIST
Round 1	CUR(T_1), CUR(T_2), Accept T_1	CUR(T_3), Accept T_3	$\emptyset$	$\emptyset$	0.826	$\{T_2\}$
Round 2	CUR(T_1)	CUR(T_2), Accept T_2, Break T_3	$\emptyset$	$\emptyset$	1.071	$\{T_3\}$
Round 3	CUR(T_1)	CUR(T_2)	CUR(T_3), Accept T_3	$\emptyset$	1.231	$\emptyset$

(c)

TABLE V
PRIORITY MATRIX OF RECEIVERS, IRSS, AND ALLOCATION ROUNDS OF 2^{nd} PHASE FROM RX TO IRS

	1^{st} Choice		2^{nd} Choice		3^{rd} Choice	
	I	Eq.(42)	I	Eq.(42)	I	Eq.(42)
R_1	I_2	0.033	I_1	0.021	I_3	0.010
R_2	I_1	0.040	I_2	0.038	I_3	0.003
R_3	I_1	0.058	I_3	0.020	I_2	0.012

(a)

	1^{st} Choice		2^{nd} Choice		3^{rd} Choice	
	R_k	Eq.(42)	R_k	Eq.(42)	R_k	Eq.(42)
I_1	R_3	0.058	R_2	0.040	R_1	0.020
I_2	R_2	0.038	R_1	0.033	R_3	0.012
I_3	R_3	0.020	R_1	0.010	R_2	0.003

(b)

	I_1	I_2	I_3	$\sum \Lambda_{T_{k^\star},I_{n^\star},R_l}$	LIST
Round 1	CUR(R_2), CUR(R_3), Accept R_3	CUR(R_2), CUR(R_1), Accept R_1	$\emptyset$	0.091	$\{R_2\}$
Round 2	CUR(R_3)	CUR(R_1), CUR(R_2), Accept R_2, Break R_1	$\emptyset$	0.096	$\{R_1\}$
Round 3	CUR(R_1), CUR(R_3), Reject R_1	CUR(R_2)	$\emptyset$	0.096	$\{R_1\}$
Round 4	CUR(R_3)	CUR(R_2)	CUR(R_1), Accept R_1	0.106	$\emptyset$

(c)

D. Convergence Analysis

The convergence of the matching algorithm can be proved following the approach in [52]. As stated in the proposed algorithm, proposers (Txs / Rxs) that have not been matched at each iteration apply to the next preferred responders (IRSs) on their priority lists. Hence, there exists competition among proposers applying for a responder. The assignment rules in the proposed algorithm indicate that the responder accepts the proposer that maximizes the sum rate. Since proposers only apply to the responder on their priority list once, the request and reject procedure ends when every proposer has matched or has been rejected by all responders. Thus it can be concluded that the proposed allocation algorithm terminates after a few iterations. Fig. 7 shows the sum rate for varying numbers of iterations with a different number of Tx / Rx pairs. It can be observed that the convergence rate decreases when the number of Tx / Rx increases since more Tx / Rx pairs need to be paired. Furthermore, when the number of IRSs increases, the convergence rate decreases in the first phase. However, the convergence rate in the second phase remains the same when the number of IRSs increases. This is because we consider that the IRSs allocated in the first phase will participate in the second phase while the rest remain inactive. The convergence of (38) is shown in the first subplot, and the second subplot demonstrates the convergence of (40). Moreover, we observe that the overall algorithm can converge very fast.

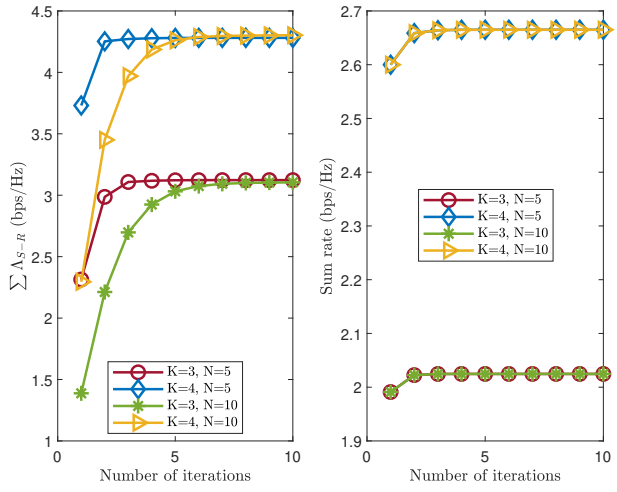


Fig. 7. Sum rate versus number of iterations for different number of Tx / Rx pairs with a network area of 20×20 m^2, $p_k = 25$ dBm, and $M = 100 \times 100$.

E. Computational Complexity Analysis

In order to reach the optimal T-I-R pairing, all possible combinations must be searched and paired with the one that maximizes the sum rate in (27), which is known as ES. The computational complexity of the ES method is $\mathcal{O}(\frac{N!L!}{(N-K)!})$. Meanwhile, the computational complexity of the PES scheme is $\mathcal{O}(\frac{N!}{(N-K)!} + L!)$ and that of the proposed matching-based scheme is $\mathcal{O}((K \times N) + (L \times L))$. Additionally, to compare the computational complexity of different methods, we take the natural logarithm of the linear computational complexity. The logarithm complexity of the ES and PES schemes is $\mathcal{O}(ln(\frac{N!L!}{(N-K)!}))$ and $\mathcal{O}(ln(\frac{N!}{(N-K)!} + L!))$, respectively, which can be simplified using logarithmic properties and Stirling's formula,

This work is licensed under a Creative Commons Attribution-NonCommercial-NoDerivatives 4.0 License. For more information, see https://creativecommons.org/licenses/by-nc-nd/4.0/

This article has been accepted for publication in IEEE Open Journal of the Communications Society. This is the author's version which has not been fully edited and content may change prior to final publication. Citation information: DOI 10.1109/OJCOMS.2024.3353173

$\ln(n!) = n\ln n$. Accordingly, the logarithm complexity of the ES is $\mathcal{O}(N\ln(N) + L\ln(L) - (N-K)\ln(N-K))$. Moreover, the complexity of the proposed scheme can be expressed in natural logarithm as $\mathcal{O}(\ln K + \ln N + \ln L)$, which is much less than that of the ES schemes.

VI. Results and Discussion

In this section, we evaluate the performance of the proposed matching-based allocation in terms of sum rate. We implemented the proposed matching-based allocation scheme using MATLAB. In the simulated scenario, explained in Section II, the transmitters, receivers, and IRSs are deployed within the network area. The carrier frequency and the channel BW are set to be $f_c = 300$ GHz and 10 GHz [53], respectively. The length and width of each IRS element is $M_x = M_y = 0.4\lambda$ [35], where λ is the wavelength. The transmit power (p_{T}), noise power density (N_0), and noise figure (NF) are 25 dBm [53], -174 dBm/Hz [53], and 10 dB [53], respectively. The AWGN noise power at each receiver is set to be $\sigma_l^2 = -N_0 + 10\log_{10}(BW) + NF = -64$ dBm. Simulation parameters, detailed in Table VI are configured based on existing works. We demonstrate how the transmission power of the transmitter influences the sum rate, the number of IRS elements, the size of the network, and the number of transmitters/receivers. Furthermore, the proposed scheme is compared to the following schemes:

- **Exhaustive Search (ES):** In the ES method, the T-I-R sum rate is utilized to find the optimal pairing by checking all possible combinations and selecting the optimal one, as in Section IV-B.
- **Partial Exhaustive Search (PES):** In the PES scheme, all the possible T-I pairing combinations are explored. Following this allocation, PES explores the optimal I-R matching, which leads to sub-optimal T-I-R matching.
- **Greedy Search (GS):** In the GS method [46], [54], each T / R selects the IRS with a higher data rate. IRSs receiving multiple proposals are randomly allocated to one of the transmitters/receivers.
- **Nearest Association (NA):** In the NA rule, each transmitter/receiver is associated with the IRS which is closest to it among all IRSs in N [24], [25].
- **Random Allocation (RA):** The RA scheme [44] randomly selects the T-I-R allocation matrix.
- **Partial Random Allocation (PRA):** The PRA scheme randomly selects the T-I allocation matrix, then also randomly selects the I-R allocation matrix.

A. Impact of the Transmission Power

We consider $N = 5$, $K = 3$, and $M = 100 \times 100$ to illustrate the impact of the transmission power on the performance matrix. Here, the sum rate increases as the transmission power increases for all the cases, as shown in Fig. 8. Moreover, the sum rate of the proposed scheme is similar to that of the PES scheme and comparable to that of the ES scheme. In addition, the sum rate of the proposed algorithm outperforms that of the NA, GS, PRA, and RA schemes.

TABLE VI
Simulation Parameters

Parameters	Values
Carrier frequency, f_c [GHz]	300
Side length of IRS elements	0.4λ [35]
Absorption coefficient, $\kappa_{abs}(f)$ $[m^{-1}]$	0.0033 [36]
Transmit power, p_{T} [dBm]	25 [53]
Noise power density, N_0 [dBm/Hz]	-174 [53]
Channel bandwidth, BW [GHz]	10 [53]
Noise figure, NF [dB]	10 [55]
Number of IRS elements, M	100×100 [55]
T_k coordinate $[m]$	$x_{\mathrm{T}}^k \sim \mathcal{U}(0\ 20)$, $y_{\mathrm{T}}^k \sim \mathcal{U}(0\ 20)$
I_n coordinate $[m]$	$x_{\mathrm{I}}^n \sim \mathcal{U}(0\ 20)$, $y_{\mathrm{I}}^n \sim \mathcal{U}(0\ 20)$, $z_{\mathrm{I}}^n \sim \mathcal{U}(0\ 5)$
R_l coordinate $[m]$	$x_{\mathrm{R}}^l \sim \mathcal{U}(0\ 20)$, $y_{\mathrm{R}}^l \sim \mathcal{U}(0\ 20)$
Avg. height of transmitters $[m]$	1
Avg. height of receivers $[m]$	1

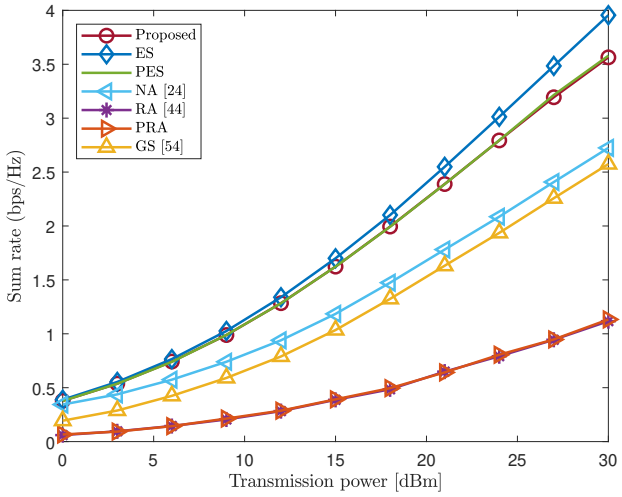


Fig. 8. Sum rate versus transmit power for a network area of 20×20 m^2 and $M = 100 \times 100$.

B. Impact of the Number of IRS Elements

To demonstrate the impact of number of reflecting elements on the performance matrix, we consider $N = 5$, $K = 3$, and $p_k = 25dBm$. The sum rate increases as M increases, as shown in Fig. 9. The reason behind this is that when M increases, the total received signal strength also increase, which ultimately improves the sum rate. Moreover, the sum-rate of the proposed algorithm is similar to that of the PES scheme and comparable to the ES method. Furthermore, the proposed scheme achieves a higher sum rate than the NA, GS, RA, and PRA, and this is due to the proper allocation of IRSs to transmitters and receivers.

C. Impact of the IRS Reflecting Efficiency

Fig. 10 demonstrates the sum rate in relation to the reflecting efficiency of IRSs. It can be observed that the reflecting efficiency of the IRS has a substantial impact on the sum rate, as expected. As κ increases the sum rate achieved by all schemes increases significantly. This is due to the less power loss caused by signal absorption at IRSs for higher κ.

This work is licensed under a Creative Commons Attribution-NonCommercial-NoDerivatives 4.0 License. For more information, see https://creativecommons.org/licenses/by-nc-nd/4.0/

This article has been accepted for publication in IEEE Open Journal of the Communications Society. This is the author's version which has not been fully edited and content may change prior to final publication. Citation information: DOI 10.1109/OJCOMS.2024.3353173

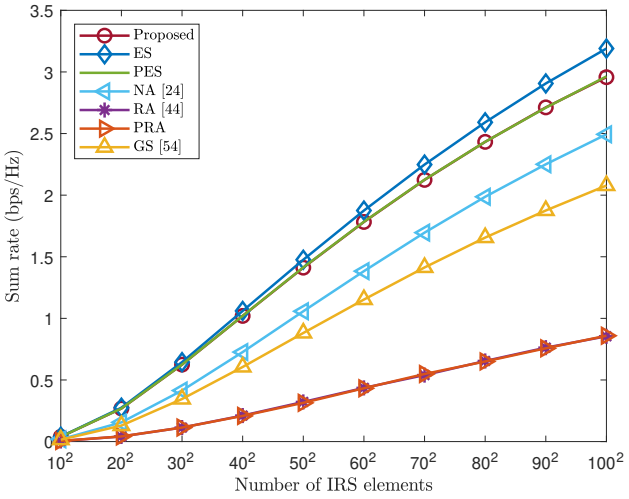


Fig. 9. Sum rate with varying number of IRS elements for a network area of 20×20 m^2 and $p_k = 25$ dBm.

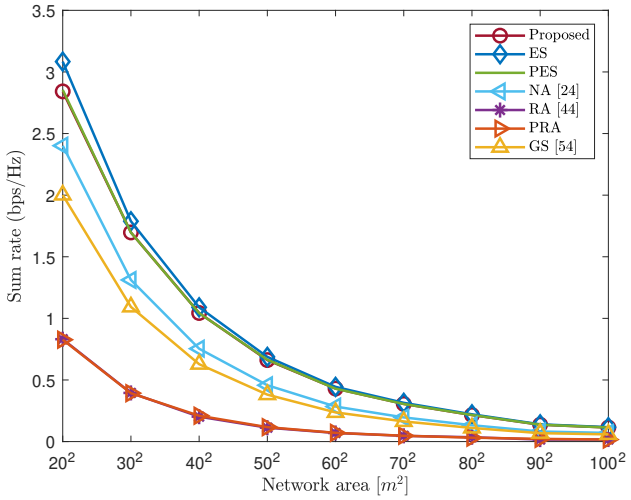


Fig. 11. Sum rate with a varying network area for $p_k = 25$ dBm and $M = 100 \times 100$.

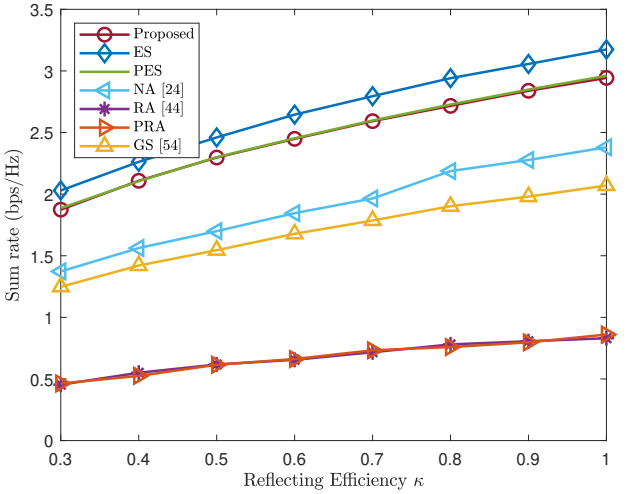


Fig. 10. Sum rate versus IRS reflecting efficiency for a network area of 20×20 m^2 and $p_k = 25$ dBm.

D. Impact of the Network Area

As shown in Fig. 11, for all schemes, the sum rate decreases as the network size increases due to the increase in the distance between the transmitters and IRSs as well as between the IRSs and receivers. Specifically, the PL is distance-dependent, and therefore the sum rate decreases against increases in the distance. Additionally, for the given network size, the sum rate achieved by the proposed scheme is identical to that of the PES scheme and superior to the sum rate of the NA, GS, PRA, and RA schemes, as depicted in Fig. 11.

E. Impact of Number of Tx/Rx and Frequency

Fig. 12 shows the impact of the number of transmitters/receivers on the sum-rate performance for 142 GHz and 300 GHz frequencies with a BW of 1 GHz and 10 GHz, respectively. The performance of the proposed scheme is superior

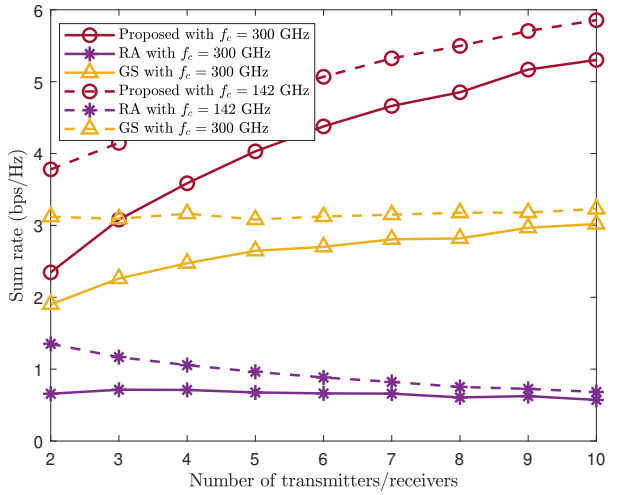


Fig. 12. Sum rate with varying number of transmitters/receivers for a network area of 20×20 m^2, $p_k = 25$ dBm, N=10, and $M = 100 \times 100$.

for both frequencies, which is due to the proper scheduling. In the meantime, the sum rate for the GS scheme remains approximately steady due to the optimal targets by proposers and the random selection of responders. However, the sum rate for the RA scheme decreases due to the increasing interference. Moreover, a higher sum-rate is achieved at 142 GHz due to lower PL.

Fig. 13 demonstrate the impact of the number of transmitters/receivers on the sum rate for two different network area. For the network area of $20 \times 20\,m^2$, the peak sum rate is achieved approximately with 10 transmitters/receivers. However, the peak sum rate is achieved approximately with 21 transmitters/receivers for the network area of $30 \times 30\,m^2$. Thus, we conclude that

This work is licensed under a Creative Commons Attribution-NonCommercial-NoDerivatives 4.0 License. For more information, see https://creativecommons.org/licenses/by-nc-nd/4.0/

This article has been accepted for publication in IEEE Open Journal of the Communications Society. This is the author's version which has not been fully edited and content may change prior to final publication. Citation information: DOI 10.1109/OJCOMS.2024.3353173

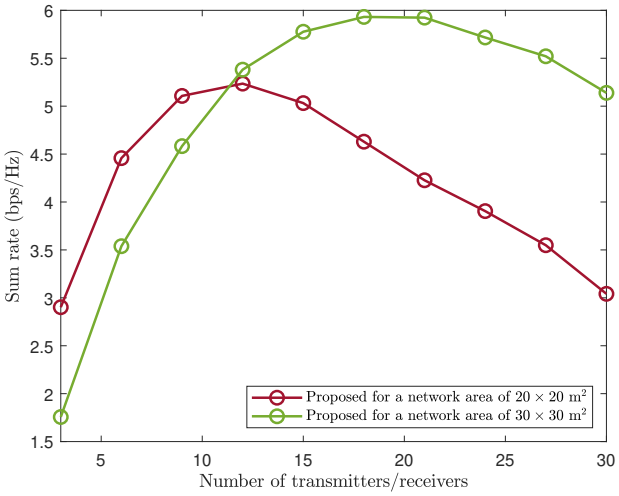


Fig. 13. Sum rate with the varying number of transmitters/receivers.

the sum rate depends on the network area and the number of transmitters/receivers.

The tradeoff between the sum rate and the computational complexity with a varying number of transmitters/receivers is elaborated in Fig. 14. It can be observed that the sum rate and the computational complexity increase with increases in the number of Tx / Rx pairs. It can be spotted from Fig. 14 that for 10 Tx / Rx pairs, the algorithm converges within 30 iterations and requires less iterations for less than 10 Tx / Rx.

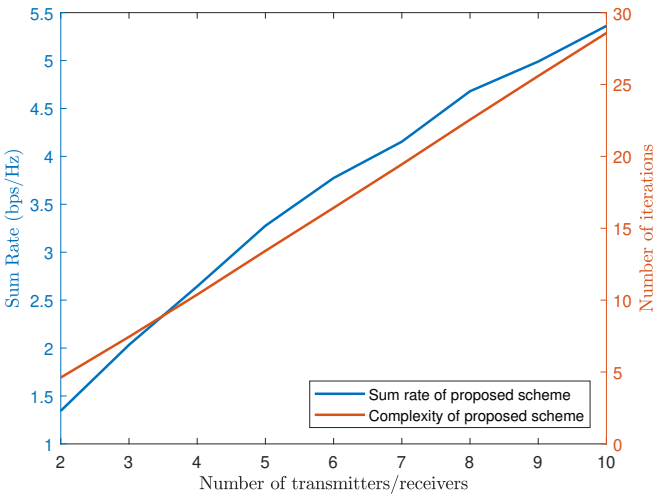


Fig. 14. A tradeoff between sum rate and complexity for different numbers of transmitters/receivers with a network area of 20×20 m^2, and $M = 100 \times 100$.

VII. Conclusions

In this paper, we considered IRS-aided THz networks with imperfect CSI, where several IRSs are deployed to assist the communication. First, we investigated the PL model for the T-I channel and I-R channel and proceeded to derive the PL model for the T-I-R cascaded channel. We then formulated the T-I-R matching problem to maximize the sum rate, an NP-hard problem. Thus, to solve the NP-hard T-I-R matching problem, we decomposed the problem into two sub-problems, which we solved with our proposed matching-based algorithm. Furthermore, we divided our proposal into two phases. In the first phase, we solved the first T-I matching sub-problem. Then, in the second phase, we achieved I-R matching using the result of the first phase. Simulation results consolidated the potential of the proposed approach for IRS-aided THz communications and demonstrated its superior performance compared to the NA, GS, PRA, and RA schemes. Moreover, provided complexity and convergence analysis verified that the computational complexity of our algorithm is lower than the ES and PES schemes. Possible future research directions based on the results obtained in this paper include the study of the mobility support model, the analysis of near-field communications, and the study of a practical amplitude and phase shift model of IRS reflecting elements.

Appendix A
Proof of Lemma 1

Considering that the incident wave from T_k is linearly polarized along the x-axis, its electric field (E-field) is presented as $\mathbf{E}_k^{\mathrm{inc}} = E_k^{\mathrm{inc}} e^{-j\kappa(y\sin\theta_k^{\mathrm{inc}} - z\cos\theta_k^{\mathrm{inc}})}\mathbf{e}_x$ [36], where E_k^{inc} [V/m] denotes the amplitude of the incident E-field and θ_k^{inc} [rad] denotes the incidence angle. We rewrite the E-field as $\mathbf{E}_k^{\mathrm{inc}} = (E_{x,k}^{\mathrm{inc}}, E_{y,k}^{\mathrm{inc}}, E_{z,k}^{\mathrm{inc}})$. Since $\mathbf{e}_x = (1,0,0)$, we obtain

$$E_{x,k}^{\mathrm{inc}} = E_k^{\mathrm{inc}} e^{-j\kappa(y\sin\theta_k^{\mathrm{inc}} - z\cos\theta_k^{\mathrm{inc}})}, \;\; E_{y,k}^{\mathrm{inc}} = E_{z,k}^{\mathrm{inc}} = 0. \quad (43)$$

Using Faraday equation, i.e., $\boldsymbol{\nabla} \times \mathbf{E}_k^{\mathrm{inc}} = -j\omega \mathbf{B}_k^{\mathrm{inc}}$ with "$\times$" being the cross product operator, we can determine the incident magnetic B-field $\mathbf{B}_k^{\mathrm{inc}} \triangleq (B_{x,k}^{\mathrm{inc}}, B_{y,k}^{\mathrm{inc}}, B_{z,k}^{\mathrm{inc}})$. Here, the left-hand side of the Faraday equation is obtained as

$$\boldsymbol{\nabla} \times \mathbf{E}_k^{\mathrm{inc}} = \left(0, \frac{\partial E_{x,k}^{\mathrm{inc}}}{\partial z}, -\frac{\partial E_{x,k}^{\mathrm{inc}}}{\partial y}\right), \quad (44)$$

where $\mathbf{e}_y = (0,1,0)$ and $\mathbf{e}_z = (0,0,1)$. The partial derivative of $E_{x,k}^{\mathrm{inc}}$ with respect to z and y are obtained as $j\kappa\cos\theta_k^{\mathrm{inc}} E_{x,k}^{\mathrm{inc}}$ and $-j\kappa\sin\theta_k^{\mathrm{inc}} E_{x,k}^{\mathrm{inc}}$, respectively. Hence, comparing the right-hand side of the Faraday equation, we obtain $B_{x,k}^{\mathrm{inc}} = 0$, $B_{y,k}^{\mathrm{inc}} = -\frac{\kappa}{\omega}\cos\theta_k^{\mathrm{inc}} E_{x,k}^{\mathrm{inc}}$, and $B_{z,k}^{\mathrm{inc}} = -\frac{\kappa}{\omega}\sin\theta_k^{\mathrm{inc}} E_{x,k}^{\mathrm{inc}}$. Hence, the magnetic B-field components of the incident wave are obtained as

$$\mathbf{B}_k^{\mathrm{inc}} = -\frac{E_k^{\mathrm{inc}}}{\eta}\left[\mathbf{e}_y\cos\theta_k^{\mathrm{inc}} + \mathbf{e}_z\sin\theta_k^{\mathrm{inc}}\right]^{-j\kappa(y\sin\theta_k^{\mathrm{inc}} - z\cos\theta_k^{\mathrm{inc}})}, \quad (45)$$

where $\eta = \omega/\kappa$. Following the analysis in [56, Section 11.3.2] and [36], the corresponding power density of the scattered E-field at R_l is obtained as

$$S_{\mathrm{T}_k,\mathrm{I}_n,\mathrm{R}_l}^{\mathrm{rfl}} = \frac{p_k \mathbb{G}_{\mathrm{T}_k}}{4\pi}\left(\frac{\frac{A}{\lambda}}{d_{\mathrm{T}_k,\mathrm{I}_{n,m}} d_{\mathrm{I}_{n,m},\mathrm{R}_l}}\right)^2 \times F(\psi_{\mathrm{T}_k,\mathrm{I}_{n,m}}, \phi_{\mathrm{I}_{n,m},\mathrm{R}_l}, \psi_{\mathrm{I}_{n,m},\mathrm{R}_l}). \quad (46)$$

This work is licensed under a Creative Commons Attribution-NonCommercial-NoDerivatives 4.0 License. For more information, see https://creativecommons.org/licenses/by-nc-nd/4.0/

This article has been accepted for publication in IEEE Open Journal of the Communications Society. This is the author's version which has not been fully edited and content may change prior to final publication. Citation information: DOI 10.1109/OJCOMS.2024.3353173

Hence, considering the molecular absorption loss in THz communication and the receive aperture $\frac{\mathbb{G}_{\mathrm{R}_l}\lambda^2}{4\pi}$, the received signal at R_l can be expressed as

$$y = \sum_{m=1}^{M_n} \sqrt{\frac{\mathbb{G}_{\mathrm{R}_l}\lambda^2}{4\pi} S^{\mathrm{rfl}}_{\mathrm{T}_k,\mathrm{I}_n,\mathrm{R}_l} \kappa_{n,m}} \sqrt{e^{-\kappa_{\mathsf{abs}}(f_c)(d_{\mathrm{T}_k,\mathrm{I}_{n,m}} + d_{\mathrm{I}_{n,m},\mathrm{R}_l})}} \times e^{-j\frac{2\pi}{\lambda}(d_{\mathrm{T}_k,\mathrm{I}_{n,m}} + d_{\mathrm{I}_{n,m},\mathrm{R}_l})} e^{j\theta_{n,m}} x_k + n_{\mathrm{R}_l}, \tag{47}$$

where $F(x,y,z) = \cos^2 x(\cos^2 y \cos^2 z + \sin^2 y)$, $\kappa_{n,m} \in (0,1]$ and $\theta_{n,m} \in [0, 2\pi)$ represent the amplitude and the PS of $\mathrm{I}_{n,m}$, respectively. Moreover, $\kappa_{\mathsf{abs}}(f)$ [m^{-1}] is the molecular absorption coefficient at the frequency of interest f [Hz]. For $f \in [275, 400]$ GHz, $\kappa_{\mathsf{abs}}(f)$ can be determined as [57]

$$\kappa_{\mathsf{abs}}(f) = y_1(f, \mu_{\mathrm{H_2O}}) + y_2(f, \mu_{\mathrm{H_2O}}) + g(f), \tag{48}$$

where $y_1(f, \mu_{\mathrm{H_2O}})$, and $y_2(f, \mu_{\mathrm{H_2O}})$, $g(f)$ are given by [57, Eq. (31), Eq. (32), Eq. (33)], respectively, $\mu_{\mathrm{H_2O}} = \frac{\phi}{100}\frac{p^*_w(T,p)}{p}$ is the volume mixing ratio of water vapor, $\phi \in [0, 100]$ is the relative humidity, and $\frac{\phi}{100}p^*_w(T,p)$ is the partial pressure of water vapor at temperature T [K] and pressure p [hPa]. Specifically, $p^*_w(T,p)$ is given by

$$p^*_w(T,p) = 6.1121\left(1.0007 + \frac{3.46}{10^6}p\right)e^{\frac{17.502(T-273.15)}{(T-32.18)}}. \tag{49}$$

Henceforth, we consider the standard atmospheric condition, where $T = 296$ K, $p = 1013.25$ hPa, and $\phi = 50$, denoting 50% humidity. Furthermore, the received signal corresponding to [37], can be expressed as

$$y = \sum_{m=1}^{M_n} \frac{\sqrt{p_k A^2 \mathbb{G}_{\mathrm{T}_k} \mathbb{G}_{\mathrm{I}_{n,m}}(-\mathbf{r}_{\mathrm{T}_k,\mathrm{I}_n,m})}}{4\pi d_{\mathrm{T}_k,\mathrm{I}_{n,m}}} \sqrt{e^{-\kappa_{\mathsf{abs}}(f_c) d_{\mathrm{T}_k,\mathrm{I}_{n,m}}}} \times \frac{\sqrt{A^2 \mathbb{G}_{\mathrm{R}_l} \mathbb{G}_{\mathrm{I}_{n,m}}(\mathbf{r}_{\mathrm{I}_{n,m},\mathrm{R}_l})}}{4\pi d_{\mathrm{I}_{n,m},\mathrm{R}_l}} \sqrt{e^{-\kappa_{\mathsf{abs}}(f_c) d_{\mathrm{I}_{n,m},\mathrm{R}_l}}} \times e^{-j\frac{2\pi}{\lambda}(d_{\mathrm{T}_k,\mathrm{I}_{n,m}} + d_{\mathrm{I}_{n,m},\mathrm{R}_l})} e^{j\theta_{n,m}} x_k + n_{\mathrm{R}_l}. \tag{50}$$

Comparing (47) and (50), we can formulate the gain of the m^{th} element of I_n as (22). This completes the proof of Lemma 1.

Appendix B
Proof of Lemma 2

In the first phase of our proposed algorithm, we find the Tx to IRS matching to maximize the pseudo quantity from Tx to IRS, which can be written as $[\overline{\mathbf{\Omega}}]_{(\mathrm{T}^\star_k,\mathrm{I}^\star_n,:)} = \arg\max_{\mathrm{T}_k,\mathrm{I}_n,:}\{\Lambda_{\mathrm{T}_k,\mathrm{I}_n,:}\}$, where $\mathrm{T}^\star_k$ and $\mathrm{T}^\star_n$ are the best possible allocation to maximize the pseudo quantity. The allocation achieved in the first phase is utilized to find the allocation matrix between the IRS and the receiver in the second phase, as $[\overline{\mathbf{\Omega}}]^\star_{\mathrm{T}_k,\mathrm{I}_n,\mathrm{R}_l} = \arg\max_{\mathrm{T}^\star_k,\mathrm{I}^\star_n,\mathrm{R}_l}\left\{\Lambda_{\mathrm{T}^\star_k,\mathrm{I}^\star_n,\mathrm{R}_l}\right\}$. The sum rate achieved by the proposed method is upper bounded by the sum rate obtained with the ES method, which can be expressed as

$$\max_{\mathrm{T}_k,\mathrm{I}_n,\mathrm{R}_l}\left\{\sum_{\mathrm{T}_k,\mathrm{I}_n,\mathrm{R}_l} R_{\mathrm{T}_k,\mathrm{I}_n,\mathrm{R}_l}\right\} \geq \max_{\mathrm{T}^\star_k,\mathrm{I}^\star_n,\mathrm{R}_l}\left\{\sum_{\mathrm{T}^\star_k,\mathrm{I}^\star_n,\mathrm{R}_l} \Lambda_{\mathrm{T}^\star_k,\mathrm{I}^\star_n,\mathrm{R}_l}\right\}, \tag{51}$$

which is equivalent to

$$\max_{\mathrm{T}_k,\mathrm{I}_n,\mathrm{R}_l}\left\{\sum_{\mathrm{T}_k,\mathrm{I}_n,\mathrm{R}_l} \log_2(1+\mathrm{SINR}_{\mathrm{T}_k,\mathrm{I}_n,\mathrm{R}_l})\right\} \geq \max_{\mathrm{T}^\star_k,\mathrm{I}^\star_n,\mathrm{R}_l}\left\{\sum_{\mathrm{T}^\star_k,\mathrm{I}^\star_n,\mathrm{R}_l} \log_2(1+\Xi_{\mathrm{T}^\star_k,\mathrm{I}^\star_n,\mathrm{R}_l})\right\}. \tag{52}$$

Since the log function is a monotonically increasing function, we have

$$\max_{\mathrm{T}_k,\mathrm{I}_n,\mathrm{R}_l}\left\{\sum_{\mathrm{T}_k,\mathrm{I}_n,\mathrm{R}_l} \mathrm{SINR}_{\mathrm{T}_k,\mathrm{I}_n,\mathrm{R}_l}\right\} \geq \max_{\mathrm{T}^\star_k,\mathrm{I}^\star_n,\mathrm{R}_l}\left\{\sum_{\mathrm{T}^\star_k,\mathrm{I}^\star_n,\mathrm{R}_l} \Xi_{\mathrm{T}^\star_k,\mathrm{I}^\star_n,\mathrm{R}_l}\right\}. \tag{53}$$

Using ideal PS, the maximum SINR can be obtained from (34). When T_k, I_n, R_l and $\mathrm{T}^\star_k$, $\mathrm{I}^\star_n$, R_l are similar, the proposed suboptimal solution gives the same rate as the ES and

$$\max_{\mathrm{T}_k,\mathrm{I}_n,\mathrm{R}_l}\left\{\sum_{\mathrm{T}_k,\mathrm{I}_n,\mathrm{R}_l} \mathrm{SINR}_{\mathrm{T}_k,\mathrm{I}_n,\mathrm{R}_l}\right\} = \max_{\mathrm{T}_k,\mathrm{I}_n,\mathrm{R}_l}\left\{\sum_{\mathrm{T}_k,\mathrm{I}_n,\mathrm{R}_l} \Xi_{\mathrm{T}_k,\mathrm{I}_n,\mathrm{R}_l}\right\}. \tag{54}$$

We consider the right side of (54), for the same allocation matrix with ideal PS using (35) and (36), $\{\Xi_{\mathrm{T}_k,\mathrm{I}_n,\mathrm{R}_l}\}$ is given in (55), at the top of next page, which is equivalent to the SINR as in (34). This completes the proof of Lemma 2.

Appendix C
Proof of Lemma 4

To prove Lemma 4, we use induction on the subsequent iteration j, where $j \geq i$. The inductive reasoning is as follows:

Initial step ($j = i$): At the i^{th} iteration, ***proposer*** P is proposing to ***responder*** R and two cases are possible according to our algorithm: (i) Either R is free, in which case R accepts the proposal from P, or (ii) R is paired with another ***proposer*** $P^\star$, and R accepts P only if R prefers P over $P^\star$. Thus, in either cases, on the i^{th} iteration, R pairs with the ***proposer*** which is at least as good as P.

Hypothesis: Assuming the claim in initial step that R pairs with the ***proposer*** which is at least as good as P is true for $j \geq i$.

Induction step: We prove the claim for the $(j+1)^{th}$ iteration. According to the above hypothesis, on j^{th} iteration, R is paired with $P^\star$, which it prefers at least as much as P. At the $(j+1)^{th}$ iteration, two cases are possible: (i) Either there are no new ***proposers*** for R, and R continue with $P^\star$, or (ii) a new ***proposer*** $P^{\star\star}$ proposes to R, and R accept the new ***proposer*** only if R prefers $P^{\star\star}$ over $P^\star$. In both cases, R pairs with the ***proposer*** it prefers at least as much as P.

Appendix D
Proof of Theorem 2

Let $\mathcal{P}$ and $\mathcal{R}$ denote the set of all proposers and responders, respectively. We consider a bipartite graph G whose vertex partitions correspond to $\mathcal{P}$ and $\mathcal{R}$, and there is an edge between a proposer $p \in \mathcal{P}$ and a responder $r \in \mathcal{R}$. We prove that there is a stable matching obtained by the proposed algorithm using contradiction as follows. Suppose that some ***proposer*** $p \in \mathcal{P}$ is

This work is licensed under a Creative Commons Attribution-NonCommercial-NoDerivatives 4.0 License. For more information, see https://creativecommons.org/licenses/by-nc-nd/4.0/

This article has been accepted for publication in IEEE Open Journal of the Communications Society. This is the author's version which has not been fully edited and content may change prior to final publication. Citation information: DOI 10.1109/OJCOMS.2024.3353173

$$\Xi_{\mathrm{T}_k,\mathrm{I}_n,\mathrm{R}_l}=\frac{\frac{p_k\lambda^2}{16\pi^2}\Big|\sum\limits_{m=1}^{M}\frac{\sqrt{\mathbb{G}_{\mathrm{T}_k}\mathbb{G}_{\mathrm{R}_l}\mathbb{G}_{\mathrm{I}_{n,m}}(-\mathbf{r}_{k,n,m})\mathbb{G}_{\mathrm{I}_{n,m}}(\mathbf{r}_{n,m,l})e^{-\kappa_{abs}(f)(d_{\mathrm{T}_k,\mathrm{I}_{n,m}}+d_{\mathrm{I}_{n,m},\mathrm{R}_l})}}}{d_{\mathrm{T}_k,\mathrm{I}_{n,m}}d_{\mathrm{I}_{n,m},\mathrm{R}_l}}\Big|^2}{\sum\limits_{\substack{j=1\\j\neq k}}^{K}\sum\limits_{i=1}^{N}p_j\big|(\widehat{\mathbf{h}}_{\mathrm{T}_j,\mathrm{I}_i})^T\mathbf{\Theta}_i\widehat{\mathbf{g}}_{\mathrm{I}_i,\mathrm{R}_l}\big|^2+\sum\limits_{j=1}^{K}\sum\limits_{i=1}^{N}p_j\big(\sigma^2_{\widetilde{g}_{\mathrm{I}_i,\mathrm{R}_l}}\big|\widehat{\mathbf{h}}^T_{\mathrm{T}_j,\mathrm{I}_i}\widehat{\mathbf{h}}_{\mathrm{T}_j,\mathrm{I}_i}\big|+\sigma^2_{\widetilde{h}_{\mathrm{T}_j,\mathrm{I}_i}}\big|\widehat{\mathbf{g}}^T_{\mathrm{I}_i,\mathrm{R}_l}\widehat{\mathbf{g}}_{\mathrm{I}_i,\mathrm{R}_l}\big|+\sigma^2_{\widetilde{h}_{\mathrm{T}_j,\mathrm{I}_i}}\sigma^2_{\widetilde{g}_{\mathrm{I}_i,\mathrm{R}_l}}\big)+\sigma^2_l}. \quad (55)$$

rejected by the best valid ***responder*** $r = best(p)$ ($r \in \mathcal{R}$) in the proposed algorithm. Furthermore, r rejects p in favor of $p^\star \in \mathcal{P}$, which r likes more $p^\star$ than p. Thus, in $r's$ priority, we have $p^\star \succ^r p$. Let us indicate this point as ***I*** (rejection point), and return to it later to drive a contradiction. According to the hypothesis that $r = best(p)$, there exists an edge between vertex p and r in G which make a stable matching Ω'. Moreover, in Ω', there is an edge between $p^\star$ and $r^\star \in R$ in a bipartite graph G. Thus, Ω' contains stable matches (p, r) and $(p^\star, r^\star)$. We now consider what the implementation of the proposed algorithms decides about the priorities of $p^\star$ between r and $r^\star$. Since ***I*** was the first event in the algorithm where any ***proposer*** was rejected by its best valid partner, at this instant the following must be true: (i) $p^\star$ has not been rejected by its $best(p^\star)$, and (ii) $p^\star$ has been rejected by every ***responder*** in the list that comes before r, since $p^\star$ is paired with r at instant ***I*** as proved in lemma 4. The above two facts jointly imply that $r \succ^{p^\star} r^\star$ in the priority list of $p^\star$. First, $best(p^\star)$ must come after r because prior hasn't rejected $p^\star$ yet, as proof in lemma 4, so $r > best(p^\star)$. Secondly, $r^\star$ is always a valid match with $p^\star$ because Ω' is a stable matching. This means $(p^\star, r)$ is an unstable match for Ω'; however, in Ω' both $p^\star$ and r prefer each other to their assigned pairs. Thus, our initial assumption that p was rejected by $best(p)$ is false, which proves that the algorithm returns the stable matching.

Now, we prove that the stability does not change when inverting the proposing order (i.e., previous ***proposer*** as ***responder*** and ***responder*** as ***proposer***). The cascaded channel from the T-to-I-to-R is composed of three parts, namely the channel from the T-to-I, the PS matrix of the IRS, and the channel from the I-to-R. In our proposed work, we consider the channel from the T-to-I in the first phase, while in the second phase, the channel from the I-to-R is considered. Moreover, channel reciprocity holds for the $\mathrm{T} \rightarrow \mathrm{I}$ and $\mathrm{I} \rightarrow \mathrm{R}$ channels [33]. Thus, inverting the proposing side doesn't affect the stability of the proposed algorithms.

REFERENCES

[1] T. S. Rappaport, Y. Xing, O. Kanhere, S. Ju, A. Madanayake, S. Mandal, A. Alkhateeb, and G. C. Trichopoulos, "Wireless communications and applications above 100 GHz: Opportunities and challenges for 6G and beyond," *IEEE access*, vol. 7, pp. 78 729–78 757, 2019.

[2] M. Z. Chowdhury, M. Shahjalal, S. Ahmed, and Y. M. Jang, "6G wireless communication systems: Applications, requirements, technologies, challenges, and research directions," *IEEE Open J. Commun. Soc.*, vol. 1, pp. 957–975, 2020.

[3] IEEE, "Ieee standard for high data rate wireless multi-media networks—amendment 2: 100 gb/s wireless switched point-to-point physical layer," pp. 1–55, 2017.

[4] Z. Wan, Z. Gao, F. Gao, M. Di Renzo, and M.-S. Alouini, "Terahertz massive MIMO with holographic reconfigurable intelligent surfaces," *IEEE Trans. Commun.*, vol. 69, no. 7, pp. 4732–4750, 2021.

[5] C. Han and I. F. Akyildiz, "Distance-aware bandwidth-adaptive resource allocation for wireless systems in the terahertz band," *IEEE Trans. Terahertz Sci. Technol.*, vol. 6, no. 4, pp. 541–553, 2016.

[6] H. Sarieddeen, M.-S. Alouini, and T. Y. Al-Naffouri, "Terahertz-band ultra-massive spatial modulation MIMO," *IEEE J. Sel. Areas Commun.*, vol. 37, no. 9, pp. 2040–2052, 2019.

[7] T. N. Do, G. Kaddoum, T. L. Nguyen, D. B. da Costa, and Z. J. Haas, "Multi-RIS-aided wireless systems: Statistical characterization and performance analysis," *IEEE Trans. Commun.*, vol. 69, no. 12, pp. 8641–8658, Dec. 2021.

[8] C. Huang, A. Zappone, G. C. Alexandropoulos, M. Debbah, and C. Yuen, "Reconfigurable intelligent surfaces for energy efficiency in wireless communication," *IEEE Trans. Wireless Commun.*, vol. 18, no. 8, pp. 4157–4170, 2019.

[9] R. Long, Y.-C. Liang, Y. Pei, and E. G. Larsson, "Active reconfigurable intelligent surface-aided wireless communications," *IEEE Trans. Wireless Commun.*, vol. 20, no. 8, pp. 4962–4975, 2021.

[10] M. Di Renzo, K. Ntontin, J. Song, F. H. Danufane, X. Qian, F. Lazarakis, J. De Rosny, D.-T. Phan-Huy, O. Simeone, R. Zhang *et al.*, "Reconfigurable intelligent surfaces vs. relaying: Differences, similarities, and performance comparison," *IEEE Open J. Commun. Soc.*, vol. 1, pp. 798–807, 2020.

[11] M. Diamanti, P. Charatsaris, E. E. Tsiropoulou, and S. Papavassiliou, "The prospect of reconfigurable intelligent surfaces in integrated access and backhaul networks," *IEEE Trans. Green Commun. Networking*, vol. 6, no. 2, pp. 859–872, 2021.

[12] Z. Yang, M. Chen, W. Saad, W. Xu, M. Shikh-Bahaei, H. V. Poor, and S. Cui, "Energy-efficient wireless communications with distributed reconfigurable intelligent surfaces," *IEEE Trans. Wireless Commun.*, 2021.

[13] R. Liu, G. Yu, and G. Y. Li, "User association for ultra-dense mmwave networks with multi-connectivity: A multi-label classification approach," *IEEE Wireless Commun. Lett.*, vol. 8, no. 6, pp. 1579–1582, 2019.

[14] J. He, K. Yu, and Y. Shi, "Coordinated passive beamforming for distributed intelligent reflecting surfaces network," in *IEEE VTC2020-Spring.* IEEE, 2020, pp. 1–5.

[15] Y. Xiu, J. Zhao, C. Yuen, Z. Zhang, and G. Gui, "Secure beamforming for multiple intelligent reflecting surfaces aided mmWave systems," *IEEE Commun. Lett.*, vol. 25, no. 2, pp. 417–421, 2020.

[16] X. Xie, C. He, X. Li, and Z. J. Wang, "Robust joint design for intelligent reflecting surfaces assisted cell-free networks," *arXiv preprint arXiv:2201.09685*, 2022. [Online]. Available: https://arxiv.org/abs/2201.09685

[17] Y. Zhang, B. Di, H. Zhang, J. Lin, C. Xu, D. Zhang, Y. Li, and L. Song, "Beyond cell-free MIMO: Energy efficient reconfigurable intelligent surface aided cell-free MIMO communications," *IEEE Trans. Cognit. Commun. Networking.*, vol. 7, no. 2, pp. 412–426, 2021.

[18] T. Hou, Y. Liu, Z. Song, X. Sun, Y. Chen, and L. Hanzo, "Reconfigurable intelligent surface aided NOMA networks," *IEEE J. Sel. Areas Commun.*, vol. 38, no. 11, pp. 2575–2588, 2020.

[19] Y. Fang, S. Atapattu, H. Inaltekin, and J. Evans, "Optimum reconfigurable intelligent surface selection for indoor and outdoor communications," *arXiv preprint arXiv:2012.11793*, 2020. [Online]. Available: https://arxiv.org/abs/2012.11793

[20] W. Mei and R. Zhang, "Cooperative beam routing for multi-IRS aided communication," *IEEE Wireless Commun. Lett.*, vol. 10, no. 2, pp. 426–430, 2020.

[21] S. Zhang and R. Zhang, "Intelligent reflecting surface aided multiple access: Capacity region and deployment strategy," in *IEEE SPAWC*, 2020, pp. 1–5.

[22] I. Yildirim, A. Uyrus, and E. Basar, "Modeling and analysis of reconfigurable intelligent surfaces for indoor and outdoor applications in future wireless networks," *IEEE Trans. Commun.*, vol. 69, no. 2, pp. 1290–1301, 2020.

[23] M. Jung, W. Saad, M. Debbah, and C. S. Hong, "On the optimality of reconfigurable intelligent surfaces (RISs): Passive beamforming, modulation,

This work is licensed under a Creative Commons Attribution-NonCommercial-NoDerivatives 4.0 License. For more information, see https://creativecommons.org/licenses/by-nc-nd/4.0/

This article has been accepted for publication in IEEE Open Journal of the Communications Society. This is the author's version which has not been fully edited and content may change prior to final publication. Citation information: DOI 10.1109/OJCOMS.2024.3353173

and resource allocation," *IEEE Trans. Wireless Commun.*, vol. 20, no. 7, pp. 4347–4363, 2021.
[24] W. Mei and R. Zhang, "Performance analysis and user association optimization for wireless network aided by multiple intelligent reflecting surfaces," *IEEE Trans. Wireless Commun.*, vol. 69, no. 9, pp. 6296–6312, 2021.
[25] H. Sun, Z. Zhao, H. Cheng, J. Lyu, X. Wang, Y. Zhang, and T. Q. Quek, "IRS-assisted RF-powered IoT networks: System modeling and performance analysis," *IEEE Trans. Wireless Commun.*, 2023.
[26] Y. Fang, S. Atapattu, H. Inaltekin, and J. Evans, "Optimum reconfigurable intelligent surface selection for wireless networks," *IEEE Trans. Commun.*, 2022.
[27] W. Khawaja, O. Ozdemir, Y. Yapici, F. Erden, and I. Guvenc, "Coverage enhancement for NLOS mmWave links using passive reflectors," *IEEE Open J. Commun. Soc.*, vol. 1, pp. 263–281, 2020.
[28] T. Noh and J. Choi, "Cell-free MIMO systems powered by intelligent reflecting surfaces," *IEEE Commun. Lett.*, 2022.
[29] E. Bjornson, O. Ozdogan, and E. G. Larsson, "Intelligent reflecting surface versus decode-and-forward: How large surfaces are needed to beat relaying?" *IEEE Wireless Commun. Lett.*, vol. 9, no. 2, pp. 244–248, Feb. 2020.
[30] Y. Liu, X. Liu, X. Mu, T. Hou, J. Xu, M. Di Renzo, and N. Al-Dhahir, "Reconfigurable intelligent surfaces: Principles and opportunities," *IEEE Commun. Surv. Tutorials*, vol. 23, no. 3, pp. 1546–1577, 2021.
[31] C. Pan, H. Ren, K. Wang, J. F. Kolb, M. Elkashlan, M. Chen, M. Di Renzo, Y. Hao, J. Wang, A. L. Swindlehurst *et al.*, "Reconfigurable intelligent surfaces for 6G systems: Principles, applications, and research directions," *IEEE Commun. Mag.*, vol. 59, no. 6, pp. 14–20, 2021.
[32] S. W. H. Shah, A. N. Mian, S. Mumtaz, A. Al-Dulaimi, I. Chih-Lin, and J. Crowcroft, "Statistical QoS analysis of reconfigurable intelligent surface-assisted D2D communication," *IEEE Trans. Veh. Technol.*, vol. 71, no. 7, pp. 7343–7358, 2022.
[33] W. Tang, X. Chen, M. Z. Chen, J. Y. Dai, Y. Han, S. Jin, Q. Cheng, G. Y. Li, and T. J. Cui, "On channel reciprocity in reconfigurable intelligent surface assisted wireless networks," *IEEE Wireless Commun.*, vol. 28, no. 6, pp. 94–101, 2021.
[34] M. Cui, Z. Wu, Y. Lu, X. Wei, and L. Dai, "Near-field MIMO communications for 6g: Fundamentals, challenges, potentials, and future directions," *IEEE Communications Magazine*, vol. 61, no. 1, pp. 40–46, Jan. 2023. [Online]. Available: https://doi.org/10.1109/mcom.004.2200136
[35] M. Najafi, V. Jamali, R. Schober, and H. V. Poor, "Physics-based modeling and scalable optimization of large intelligent reflecting surfaces," *IEEE Trans. Commun.*, vol. 69, no. 4, pp. 2673–2691, 2020.
[36] K. Dovelos, S. D. Assimonis, H. Quoc Ngo, B. Bellalta, and M. Matthaiou, "Intelligent reflecting surfaces at terahertz bands: Channel modeling and analysis," in *ICC Workshops*. IEEE, Jun. 2021, pp. 1–6.
[37] Y. U. Ozcan, O. Ozdemir, and G. K. Kurt, "Reconfigurable intelligent surfaces for the connectivity of autonomous vehicles," *IEEE Trans. Veh. Technol.*, vol. 70, no. 3, pp. 2508–2513, 2021.
[38] Ö. Özdogan, E. Björnson, and E. G. Larsson, "Intelligent reflecting surfaces: Physics, propagation, and pathloss modeling," *IEEE Wireless Commun. Lett.*, vol. 9, no. 5, pp. 581–585, 2019.
[39] X. Hu, C. Zhong, and Z. Zhang, "Angle-domain intelligent reflecting surface systems: Design and analysis," *IEEE Trans. Commun.*, vol. 69, no. 6, pp. 4202–4215, 2021.
[40] T. L. Nguyen, T. N. Do, G. Kaddoum, D. B. da Costa, and Z. J. Haas, "Channel characterization for RIS-aided terahertz communications: A stochastic approach," *IEEE Wireless Commun. Lett.*, vol. 11, no. 9, pp. 1890–1894, 2022.
[41] S. W. Ellingson, "Path loss in reconfigurable intelligent surface-enabled channels," in *2021 IEEE PIMRC*. IEEE, 2021, pp. 829–835.
[42] W. Ni, X. Liu, Y. Liu, H. Tian, and Y. Chen, "Resource allocation for multi-cell IRS-aided NOMA networks," *IEEE Trans. Wireless Commun.*, vol. 20, no. 7, pp. 4253–4268, 2021.
[43] C. A. Balanis, *Advanced engineering electromagnetics*. John Wiley & Sons, 2012.
[44] J. Cui, Y. Liu, Z. Ding, P. Fan, and A. Nallanathan, "Optimal user scheduling and power allocation for millimeter wave NOMA systems," *IEEE Trans. Wireless Commun.*, vol. 17, no. 3, pp. 1502–1517, 2017.
[45] A. Alizadeh and M. Vu, "Load balancing user association in millimeter wave MIMO networks," *IEEE Trans. Wireless Commun.*, vol. 18, no. 6, pp. 2932–2945, 2019.
[46] S. Sun, F. Yang, and J. Song, "Sum rate maximization for intelligent reflecting surface-aided visible light communications," *IEEE Communications Letters*, vol. 25, no. 11, pp. 3619–3623, 2021.
[47] M. N. Jung, C. Kirches, and S. Sager, "On perspective functions and vanishing constraints in mixed-integer nonlinear optimal control," in *Facets of combinatorial optimization*. Springer, 2013, pp. 387–417.
[48] S. Burer and A. N. Letchford, "Non-convex mixed-integer nonlinear programming: A survey," *Surveys in Operations Research and Management Science*, vol. 17, no. 2, pp. 97–106, 2012.
[49] F. Fang, H. Zhang, J. Cheng, and V. C. Leung, "Energy-efficient resource allocation for downlink non-orthogonal multiple access network," *IEEE Trans. Commun.*, vol. 64, no. 9, pp. 3722–3732, 2016.
[50] Z. Wang, L. Liu, and S. Cui, "Channel estimation for intelligent reflecting surface assisted multiuser communications: Framework, algorithms, and analysis," *IEEE Trans. Wireless Commun.*, vol. 19, no. 10, pp. 6607–6620, 2020.
[51] D. Gale and L. S. Shapley, "College admissions and the stability of marriage," *The American Mathematical Monthly*, vol. 69, no. 1, pp. 9–15, 1962.
[52] S. Shamaei, S. Bayat, and A. M. A. Hemmatyar, "Interference management in d2d-enabled heterogeneous cellular networks using matching theory," *IEEE Trans. Mob. Comput.*, vol. 18, no. 9, pp. 2091–2102, 2018.
[53] H. Zhang, Y. Duan, K. Long, and V. C. Leung, "Energy efficient resource allocation in terahertz downlink NOMA systems," *IEEE Trans. Commun.*, vol. 69, no. 2, pp. 1375–1384, 2020.
[54] Y. Xu and S. Mao, "User association in massive MIMO hetnets," *IEEE Syst. J.*, vol. 11, no. 1, pp. 7–19, 2015.
[55] M. Rahim, G. Kaddoum, and T. N. Do, "Joint devices and IRSs association for terahertz communications in industrial IoT networks," *IEEE Trans. Green Commun. Networking*, pp. 1–1, 2023.
[56] C. A. Balanis, *Antenna theory: analysis and design*. Wiley-Interscience, 2005.
[57] S. Tarboush, H. Sarieddeen, H. Chen, M. H. Loukil, H. Jemaa, M.-S. Alouini, and T. Y. Al-Naffouri, "TeraMIMO: A channel simulator for wideband ultra-massive MIMO Terahertz communications," *IEEE Trans. Veh. Technol.*, vol. 70, no. 12, pp. 12 325–12 341, Dec. 2021.



Muddasir Rahim received his B.S. and M.S. degree in Electrical (Telecommunication) Engineering from COMSATS University Islamabad, Pakistan in March. 2016 and September 2020, respectively. He is currently a Ph.D. Scholar at École de Technologie Supérieure (ÉTS), Université du Québec, Montréal, Canada. He was a Research Assistant in the Department of Electrical and Computer Engineering at COMSATS University Islamabad, Pakistan, from 2019 to 2020. His research interests include cognitive radio networks, device-to-device communication, wireless sensor networks, intelligent reconfigurable surface, matching theory, and terahertz communications.



Thanh-Luan Nguyen received the B.S. degree (with honors) from the Ho Chi Minh City University of Technology and Education, Vietnam, in 2016. He is currently a graduate student at the École de Technologie Supérieure (ÉTS), Université du Québec, Montréal, Canada. He has authored and co-authored over 10 ISI-Indexed journals with over 200 citations. His research interests include wireless communication channels, energy harvesting, reconfigurable intelligent surfaces, and other emerging wireless technologies.

This work is licensed under a Creative Commons Attribution-NonCommercial-NoDerivatives 4.0 License. For more information, see https://creativecommons.org/licenses/by-nc-nd/4.0/

This article has been accepted for publication in IEEE Open Journal of the Communications Society. This is the author's version which has not been fully edited and content may change prior to final publication. Citation information: DOI 10.1109/OJCOMS.2024.3353173



Prof. Georges Kaddoum (Senior Member, IEEE) received the bachelor's degree in electrical engineering from the École Nationale Supérieure de Techniques Avancées (ENSTA Bretagne), Brest, France, the M.S. degree in telecommunications and signal processing (circuits, systems, and signal processing) from the Université de Bretagne Occidentale and Telecom Bretagne (ENSTB), Brest, in 2005, and the Ph.D. degree (High Hons.) in signal processing and telecommunications from the National Institute of Applied Sciences (INSA), University of Toulouse, Toulouse, France, in 2009. He is currently a Professor, research director of the Resilient Machine Learning Institute (ReMI), and the Tier 2 Canada Research Chair of the École de Technologie Supérieure (ÉTS), Université du Québec, Montréal, Canada. He has published over more than 300 journals, conference papers, two chapters in books, and has eight pending patents. His recent research interests include wireless communication networks, tactical communications, resource allocations, and network security. He received the best papers awards at the 2014 IEEE International Conference on Wireless and Mobile Computing, Networking, Communications (WIMOB), at the 2017 IEEE International Symposium on Personal Indoor and Mobile Radio Communications (PIMRC), and at the 2023 IEEE International Wireless Communications & Mobile Computing Conference (IWCMC). Moreover, he received IEEE Transactions on Communications Exemplary Reviewer Award, in 2015, 2017, and 2019. In addition, he received the Research Excellence Award of the Université du Québec, in 2018. In 2019, he received the Research Excellence Award from ÉTS in recognition of his outstanding research outcomes. He also won the 2022 IEEE Technical Committee on Scalable Computing (TCSC) Award for Excellence (Middle Career Researcher). Lastly, he has received the prestigious 2023 MITACS Award for Exceptional Leadership. Prof Kaddoum served as an Associate Editor for IEEE Transactions on Information Forensics and Security and IEEE Communications Letters. He is currently serving as an Area Editor for the IEEE Transactions on Machine Learning in Communications and Networking and an editor for the IEEE Transactions on Communications.



Tri Nhu Do is an Assistant Professor of Telecommunications in the Department of Electrical Engineering at Polytechnique Montréal, Québec, Canada. He was born in Da Nang, Vietnam. In 2012, he received a bachelor's degree in Electronics and Telecommunications Engineering from the Posts and Telecommunications Institute of Technology in Vietnam. In 2015 and 2018, he received a master's degree and a Ph.D. degree, respectively, in Electronics and Computer Engineering from Hongik University in South Korea. From 2017 to 2018, he worked as a Teaching Associate in the Department of Software and Communications Engineering at Hongik University. In 2019, he was a Research Associate in the Department of Computer Science at the University of Texas at Dallas, TX, USA. From 2020 to Sep. 2023, he was a Postdoctoral Research Fellow at the Resilient Machine Learning Institute (ReMI) at École de Technologie Supérieure (ÉTS), Université du Québec, Montréal, Canada.

This work is licensed under a Creative Commons Attribution-NonCommercial-NoDerivatives 4.0 License. For more information, see https://creativecommons.org/licenses/by-nc-nd/4.0/